Hao Zhang, Dennis Kaczmarek, Charlotte Rudolph, Steffen Schmitt, Nina Gaiser, Patrick Oßwald, Thomas Bierkandt, Tina Kasper, Burak Atakan, Katharina Kohse-Höinghaus, Dimethyl ether (DME) and dimethoxymethane (DMM) as reaction enhancers for methane: combining flame experiments with model-assisted exploration of a polygeneration process, Combustion and Flame 237 (2022) 111863.

The original publication is available at www.elsevier.com

https://doi.org/10.1016/j.combustflame.2021.111863

Dimethyl ether (DME) and dimethoxymethane (DMM) as reaction enhancers for methane: combining flame experiments with model-assisted exploration of a polygeneration process

Hao Zhang [a,d,1,*], Dennis Kaczmarek [b,1], Charlotte Rudolph [c,1], Steffen Schmitt [a], Nina Gaiser [d], Patrick Oßwald [d], Thomas Bierkandt [d], Tina Kasper [b], Burak Atakan [c], Katharina Kohse-Höinghaus [a]

[1.] These authors contributed equally to this work.

[a.] *Department of Chemistry, Bielefeld University, Universitätsstraße 25, 33615 Bielefeld, Germany*

[b.] *Institute for Combustion and Gas Dynamics, Reactive Flows, University of Duisburg-Essen, Lotharstraße 1, 47057 Duisburg, Germany*

[c.] *Institute for Combustion and Gas Dynamics, Thermodynamics, University of Duisburg-Essen, Lotharstraße 1, 47057 Duisburg, Germany*

[d.] *Institute of Combustion Technology, German Aerospace Center (DLR), Pfaffenwaldring 38-40, 70569 Stuttgart, Germany*

*Corresponding author:
Dr. Hao Zhang
E-mail: zhanghao900320@gmail.com, Hao.Zhang@uni-bielefeld.de
Tel: +86 15105813531

Supplemental Materials are available:

Supplemental Material 1 (SM1): Experimental data, calibration methods, and sources of electron ionization cross-sections; temperature profiles.

Supplemental Material 2 (SM2): Further information on model and validation under different conditions, flame speciation, and engine simulations.

Supplemental Material 3 (SM3): Kinetics, thermodynamics, and transport property files of the PolyMech2.1 model

Abstract

The potential of dimethyl ether (DME) and dimethoxymethane (DMM), representatives of the attractive oxymethylene ether (OME) alternative fuel family, are explored here as reactivity enhancers for methane-fueled polygeneration processes. Typically, such processes that can flexibly generate power, heat, or chemicals, operate under fuel-rich conditions in gas turbines or internal combustion engines. To provide a consistent basis for the underlying reaction mechanisms, it is recognized that speciation data for the DME/CH_4 fuel combination are available for such conditions while such information for the DMM/CH_4 system is largely lacking. In addition, it should be noted that a detailed speciation study in flames, *i.e.*, combustion systems involving chemistry and transport processes over a large temperature range, is still missing in spite of the potential of such systems to provide extended species information. In a systematic approach using speciation with electron ionization molecular-beam mass spectrometry (EI-MBMS), we thus report, as a first step, investigation of six fuel-rich premixed flames of DME and DMM and their blends with methane with special attention on interesting chemicals. Secondly, a comprehensive but compact DME/DMM/CH_4 model (PolyMech2.1) is developed based on these data. This model is then examined against available experimental data under conditions from various facilities, focusing preferentially on elevated pressure and fuel-rich conditions. Comparison with existing literature models is also included in this evaluation. Thirdly, an analysis is given on this basis, *via* the extensively tested PolyMech2.1 model, for assumed polygeneration conditions in a homogeneous charge compression ignition (HCCI) engine environment. The main interest of this model-assisted exploration is to evaluate whether addition of DME or DMM in a polygeneration process can lead to potentially useful conditions for the production of syngas or other chemicals, along with work and heat.

Results in the flames show that high syngas yields, *i.e.*, up to ~78% for CO and ~35% for H_2, can be obtained in their burnt gases. From the large number of intermediates detected, predominantly acetylene, ethylene, ethane, and formaldehyde show yields of 2.1%-4.4% (C_2 hydrocarbons) and 3.4%-8.7% (CH_2O), respectively. Also, methanol and methyl formate show comparably high yields of up to 0.6%-6.7% in the flames with DMM, which is 1-2 orders of magnitude higher than in those with DME as the additive. In the modeling-assisted exploration of the engine process, the PolyMech2.1 model is seen to perform at significantly reduced computational costs compared to a recently validated model without sacrificing the prediction performance. Promising conditions for the assumed polygeneration process using fuel combinations in the DME/DMM/CH_4 system are identified with attractive syngas yields of up to 77% together with work and heat output at exergetic efficiencies of up to 89% with DME.

Keywords: Dimethyl ether, dimethoxymethane, methane, premixed flames, polygeneration, engine simulation, syngas production

1. Introduction

The limited availability of fossil fuels and efforts to reduce CO_2 emissions motivate the development of flexible and efficient energy conversion strategies. Regarding worldwide transformation efforts towards renewable energy, there is a strong demand for strategies of effectively storing fluctuating electricity. Polygeneration processes that can provide different types of energy flexibly depending on the respective demand have thus gained increasing interest [1-3]. Recent research has shown that a fuel-rich operated gas turbine or a homogeneous charge compression ignition (HCCI) engine can simultaneously – but variably – provide work, heat, and useful chemicals such as syngas, unsaturated, or partially oxidized hydrocarbons with high exergetic efficiency [1, 2, 4-7]. In these systems, methane as the main constituent of natural gas and biogas, is often used as the main fuel, assuming that it will continue to play an important role in the energy sector in the near future and will also be sufficiently available [8]. The conversion of methane towards valuable chemicals in such polygeneration systems is favored at high equivalence ratios (typically Φ >2) beyond those typical for traditional combustion, at moderate temperatures, and at high pressures [9]. However, methane is comparably inert and features poor ignition properties, which poses challenges in an HCCI process [2, 8, 10]. To this end, ignition-enhancing additives are typically needed to increase reaction rates already at moderate temperatures [2, 8].

Apart from ozone and reactive hydrocarbons like *n*-heptane [11-13], small representatives of the oxymethylene ether (OME_n) fuel family with molecular structure of $CH_3O(CH_2O)_nCH_3$ have also attracted recent attention as reactivity enhancers [14]. OME_n, with generally high cetane number, high oxygen content, absence of C–C bonds and therefore low sooting propensity, are considered as potential electric fuels (e-fuels) that can be synthesized sustainably [15-18]. To comprehensively assess the application potential of a respective OME_n/methane polygeneration system, detailed knowledge and deep understanding of the combustion behavior of such fuel mixtures and the underlying kinetics are a prerequisite.

Available research on the combustion of OME_n/methane mixtures is almost exclusively limited to the particular case of OME_n with n=0, *i.e.*, dimethyl ether (DME, CH_3OCH_3). Investigations of the DME/CH_4 system [6, 7, 10, 19-29] have targeted global combustion parameters such as flame speed and ignition delay times (IDTs) as well as speciation in plug-flow reactors (PFRs), shock tubes (STs), and rapid compression machines (RCMs). The wide range of conditions covered includes some polygeneration-relevant ones, as

evident from Fig. 1.

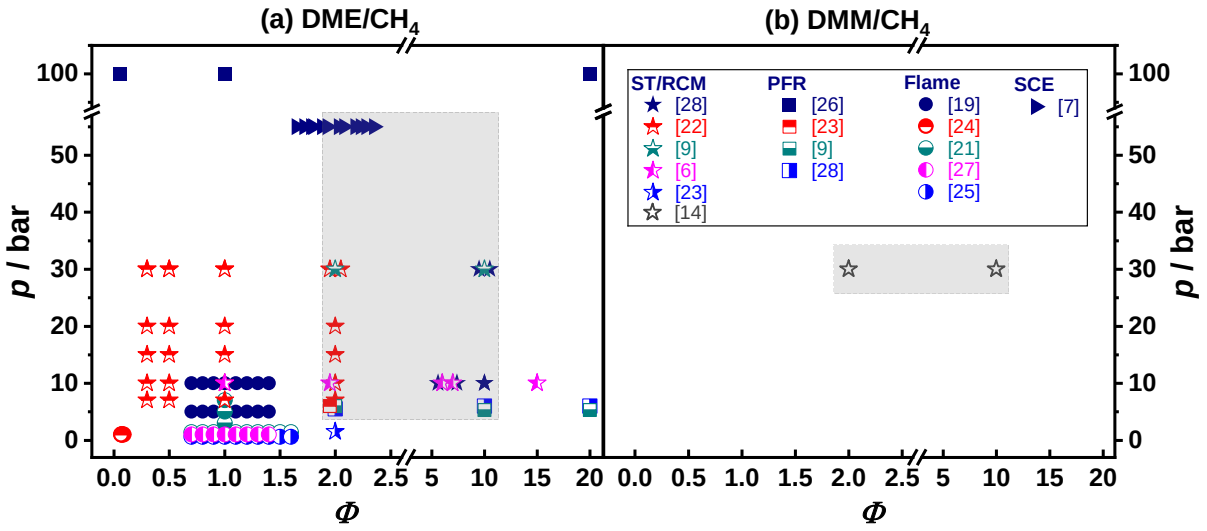

Fig. 1. Summary of literature experimental studies on the combustion of DME/CH_4 (a) and DMM/CH_4 (b) mixtures (ST: Shock tube; RCM: Rapid compression machine; PFR: Plug-flow reactor; SCE: Single-cylinder engine). For better visualization, the overlapping points in (a) have been slightly separated, *i.e.*, at Φ=0.7-1.4/p=1 bar [27], Φ=0.7-1.6/p=1 bar [21, 25], Φ=2.0/p=6 bar [9, 23, 28], Φ=2.0/p=10 bar [6, 22], Φ=2.0/p=30 bar [9, 22], Φ=6.0, 7.0/p=10 bar [6, 28], Φ=10.0/p=30 bar [9, 28], and Φ=10.0, 20.0 /p=6 bar [9, 28]. Studies under polygeneration-relevant conditions are highlighted in the boxes.

DME addition shows enhancing effects on both, the reactivity [20, 22, 23, 26, 28-30] and flame speed/stability of methane [19, 21, 25, 27, 31, 32], as well as inhibiting effects on polycyclic aromatic hydrocarbon (PAH) and/or soot formation in non-premixed methane flames [24, 33]. With respect to larger OME_n fuels as additive to methane, the only available report is, to our knowledge, by Herzler et al. [14], who investigated the IDTs and combustion products of methane mixtures with OME_1, *i.e.*, dimethoxymethane (DMM, $CH_3OCH_2OCH_3$), in a high-pressure ST. While Fig. 1 shows, as a contrast to DME addition, the very limited amount of data involving DMM, the authors [14] found also DMM to be an effective reactivity enhancer for methane. Furthermore, we are not aware of a detailed speciation study in flames of DME/methane or DMM/methane. Flames normally cover a larger range of temperature involving the chemistry at both high and low temperature, as well as the transition regime and reaction times relevant to engines. They also include transport processes that are involved in the HCCI engine conditions but cannot be considered in the reported PFR, ST, and RCM systems [6, 7, 10, 14, 19-29]. Moreover, in comparison to these facilities, the studied flame configuration can provide information on an extended species pool (*e.g.*, radicals [34, 35]). Therefore, such flame speciation measurements are highly valuable for understanding the combustion characteristics and the underlying kinetics [36]. They can also provide complementary data to

the existing low-temperature and high-pressure literature data for a critical inspection and development of comprehensive models for the fuel blends, which cannot be applied with confidence to a practical polygeneration system without validation against a wide range of laboratory-scale combustion experiments. Furthermore, the alternative concept of stratified combustion in engines with spark ignition could also be of interest for polygeneration processes, requiring the study at a broad range of equivalence ratios and temperatures that are prevailing in stratified combustion.

In the present work, we therefore address the combustion chemistry of mixtures of DME (OME_0) and DMM (OME_1) with methane in low-pressure flames with an aim to understand and compare their reaction properties and to explore the potential of both additives in a CH_4-fueled polygeneration process. It is noteworthy that despite of the wealth of insight into single-fuel combustion [37-42] and the fact that several recent models are available for DME or DMM, including the Burke DME model [22] (or AramcoMech 3.0 [43]), and the Jacobs DMM model [44], questions remain whether these OME_n models can properly describe the flame chemistry of their fuel blends with methane. For polygeneration-relevant conditions, a comprehensive and widely validated model appears desirable that can describe the DME/DMM/CH_4 system in appropriate detail yet with attractive computational cost suitable for implementation into computational fluid dynamics (CFD) codes, so that it could be used for an efficient modeling-assisted evaluation or development of a HCCI engine-based polygeneration process.

With respect to this goal, we have investigated laminar premixed low-pressure fuel-rich flames of DME, DMM, and their blends with methane using electron ionization molecular-beam mass spectrometry (EI-MBMS) to obtain detailed quantitative speciation data of major species and intermediates. Six flames with different amounts of DME or DMM from 100% to 20% (mole percentage) and equivalence ratios (Φ) of 1.4 and 1.7 were measured to provide data in an appreciable range of conditions for a critical inspection of models. Special attention was paid to the formation of useful chemicals including syngas, unsaturated and partially oxidized hydrocarbons, to provide fundamental insight for a potential polygeneration process. On the basis of these experiments, a relatively compact model PolyMech2.1 was then developed, extending the previous PolyMech model for DME/CH_4 [9, 28] to comprehensively describe the present DME/DMM/CH_4 system. Importantly, in addition to the obtained flame data, this PolyMech2.1 was validated over a large range of polygeneration-relevant conditions (p=6-100 bar, Φ=2-20) in different combustion facilities, so that it can be applied with confidence as a predictive tool for a polygeneration process. It was then deemed interesting

to assess, on the basis of this extensive validation, whether apparently useful behavior under more fundamental conditions could permit an explorative assessment of the suitability of the additives for prototypical HCCI conditions. To this end, a model-based parameter study and exergy analysis was performed to identify interesting conditions for the production of target chemicals (*e.g.*, syngas) and output of work and heat in an assumed HCCI engine polygeneration process.

2. Experiments

Laminar premixed flames were stabilized on a vertically movable homemade flat bronze burner (63.82 mm diameter, water-cooled to 333 K) and investigated using the EI-MBMS setup at Bielefeld University. Conditions for the investigated six flames are tabulated in Table 1. They comprise neat fuels of DME and DMM, fuel mixtures of 62% DME/38% CH_4 and 50% DMM/50% CH_4 at Φ=1.7, as well as 20% DME/80% CH_4 and 20% DMM/80% CH_4 at Φ=1.4. Note that equivalence ratios and additive amounts are not identical for the DME and DMM cases depending on the attainable range of stable flame conditions. Since the flame structure and chemistry of methane have been extensively investigated and well understood [42, 45-48], neat CH_4 flames were not measured in this study. All flames here were stabilized at the same pressure (p) of 40 mbar with oxygen as the oxidizer and an argon dilution of 50%. The total inlet flow rate was kept at 3.8 slm (standard liter per minute at p=1 atm, T=273 K), yielding a cold gas velocity of around 61 cm s^{-1} (40 mbar, 333 K).

Table 1. Experimental conditions of the investigated laminar premixed flames. The inlet mass flow and carbon flux are normalized to the cross-sectional area of the burner.

Fuel blends (mol%)	***x*(CH4)**	***x*(DME)**	***x*(DMM)**	***x*(O2)**	***x*(Ar)**	***Φ***	**C/O**	**Mass flow (g cm^{-2} s^{-1})**	**Carbon flux (mol cm^{-2} s^{-1})**
100DME	-	0.181	-	0.319	0.500	1.7	0.442	$3.395 \cdot 10^{-3}$	$3.195 \cdot 10^{-5}$
62DME/38CH4	0.074	0.122	-	0.304	0.500	1.7	0.438	$3.221 \cdot 10^{-3}$	$2.819 \cdot 10^{-5}$
20DME/80CH4	0.156	0.039	-	0.305	0.500	1.4	0.359	$3.002 \cdot 10^{-3}$	$2.062 \cdot 10^{-5}$
100DMM	-	-	0.149	0.351	0.500	1.7	0.447	$3.750 \cdot 10^{-3}$	$3.951 \cdot 10^{-5}$
50DMM/50CH4	0.090	-	0.090	0.320	0.500	1.7	0.442	$3.397 \cdot 10^{-3}$	$3.196 \cdot 10^{-5}$
20DMM/80CH4	0.147	-	0.037	0.316	0.500	1.4	0.366	$3.108 \cdot 10^{-3}$	$2.278 \cdot 10^{-5}$

The gas flows of DME, methane, and oxygen (Linde AG, ≥99.5%) were regulated by calibrated mass flow controllers (MKS Instruments, ~5% uncertainty), and that of argon (Linde AG, ≥99.996%) was controlled by Coriolis flow meters (Bronkhorst). Liquid DMM (Sigma-Aldrich, ≥99.0%) was evaporated in a standard vaporizer system (Bronkhorst/CEM) with argon as the carrier gas, and then mixed with the gas mixture before

flowing into the burner.

The EI-MBMS setup used to detect stable and reactive species has already been described before [49, 50] and only important aspects will be presented here. Gas samples as a function of position were extracted from the flame *via* a quartz nozzle (~500 μm orifice, 25° opening angle) and expanded into the first pumping stage (10^{-4} mbar) to rapidly quench further reactions, and then guided through a copper skimmer into the ionization chamber of the mass spectrometer (10^{-6} mbar). A two-stage Wiley-McLaren ion source with a reflectron time-of-flight (TOF) detection unit (mass resolution $m/\Delta m \approx 3900$) enables unambiguous determination of the elemental composition of C/H/O species. The electron energy used for ionization was kept as low as possible while ensuring good signal-to-noise ratio, to minimize undesired fragmentation. Specifically, nominal electron energies of 10.5 and 12 eV for intermediate species detection and 15 eV for major species detection were chosen.

The data evaluation procedures followed those reported previously [49]. Fragmentation corrections of the integrated mass signals as a function of height above the burner *h* were performed for possible fragment ions originating from the fuel and selected important intermediate species (methane in neat DME or DMM flames; acetylene, ethylene, ethane, methanol, propene, and methyl formate in all flames), relying on independent cold-gas measurements for these species. Moreover, isotope corrections for ^{13}C and ^{18}O isotopes were also performed. The corrected mass signal S_i of a species *i* can be expressed as a function of its mole fraction x_i, as given in Eq. (1):

$$S_i = x_i \cdot c \cdot \varphi \cdot SW \cdot D_i \cdot FKT(h) \cdot \int \sigma_i(\tau) \cdot f(E-\tau) d\tau \quad (1)$$

Here, c is an instrument factor, φ is the number of electrons, SW is the number of sweeps, D_i is the mass discrimination factor, $FKT(h)$ is a position- and temperature-dependent sampling function, and $\int \sigma_i(\tau) \cdot f(E-\tau) d\tau$ corresponds to convolution of the energy distribution of the electrons with the energy-dependent ionization cross section, where τ is the integration variable. D_i has been investigated previously by Schenk et al. [50] and these factors were set to unity for all species except H_2 that was internally calibrated as described below. Quantification with Eq. (1) can be simplified by using an energy- and species-dependent calibration factor $k_{i/Ar}$ relative to an inert species, which is argon in this case:

$$\frac{S_i}{S_{Ar}} = \frac{x_i}{x_{Ar}} \cdot \frac{D_i \cdot \int \sigma_i(\tau) \cdot f(E-\tau) d\tau}{D_{Ar} \cdot \int \sigma_{Ar}(\tau) \cdot f(E-\tau) d\tau} = \frac{x_i}{x_{Ar}} \cdot k_{i/Ar}(E) \quad (2)$$

Calibration factors of major species (DME, DMM, CH_4, O_2, H_2O, CO, CO_2, H_2) were determined relying on an internal calibration procedure based on the element balances of C, H, O and the derived calibration factor of CO/CO_2 from direct measurement of an $Ar/CO/CO_2/H_2$ cold-gas mixture with known composition [50]. Calibration factors of important intermediates, *i.e.*, methane (only for 100DME and 100DMM flames), acetylene, ethylene, ethane, methanol, propene, and methyl formate, were obtained by direct calibration measurements for the respective cold-gas mixtures with known compositions. For the remaining detected species, calibration factors were estimated either using the relative ionization cross section method (RICS) [51] or the convolution of the literature ionization cross sections with the known energy distribution of the ionization electrons [50]. The resulting uncertainties for mole fractions of respective species are estimated to be within 30% for the internal calibration and direct calibration procedures, and within a factor of 2-4 for the RICS and convolution procedures depending on the available EI cross-section data from literature. In cases where none of the above calibration methods are feasible, the qualitative species profiles are presented in terms of signal intensities normalized by the Ar signal, which is directly proportional to the species mole fraction according to Eq. (1). All experimental data including species-related information on the respective calibration method are tabulated in Supplemental Material 1 (SM1).

Flame temperature profiles were obtained following the sampling-rate-based procedure described by Struckmeier et al. [52], which relies on the pressure in the first pumping stage and a calibration temperature in the exhaust gas zone. In this study, the calibration temperature was measured independently without the sampling nozzle by using a type R thermocouple (diameter 0.45 mm) coated with SiO_2. A radiation correction was performed following previously reported procedure [53, 54] based on a known DME flame temperature profile obtained by OH planar laser-induced fluorescence (PLIF) as described in [55]. Temperature profiles of the six investigated flames are available in SM1 and were used as input for the chemical kinetics simulations. The uncertainty in the temperature measurement is estimated to be ±10%, which is within the typical range given by Egolfopoulos et al. [56]. To evaluate the sensitivity of the simulation results to temperature, simulations of investigated flames with reduced (-10%) and increased (+10%) temperatures were performed with the PolyMech2.1 model developed in this work (see Section 3.1); selected results are given in Section S-I in SM2. Changing the temperature within this complete uncertainty range shows no

significant influence on the mole fractions of the main species and most intermediates. Although higher deviations (up to a factor of two depending on the mixtures, conditions, and species) were observed at reduced temperatures for species that are very sensitive to temperature, *i.e.*, CH_4 and C_3H_8 for most of the flames and DME and CH_3OH for the DMM(/CH_4) flames, the conclusions drawn in this work are not affected.

The yield of products was calculated on the basis of H atoms for H_2 and H_2O and of C atoms for C-containing products, according to the formula:

$$Y_i = \frac{x_i \cdot \dot{n}_{out} \cdot \text{number of C or H atoms in product species } i}{\sum_{\text{Reactants}} x_j \cdot \dot{n}_{in} \cdot \text{ number of C or H atoms in reactant species } j} \quad (3)$$

where $\dot{n}_{in}$ and $\dot{n}_{out}$ are the total mole flow rates of the inlet reactants and outlet products, respectively. With respect to the flame data evaluation, the $\dot{n}_{out}$ at height h above the burner was derived from the ratio of the Ar mole flow rate to the Ar mole fraction at h.

3. Modeling and polygeneration test cases

A comprehensive but still compact DME/DMM/CH_4 chemical kinetic model (PolyMech2.1) was developed in this study with a special focus on engine-based polygeneration processes. Simulations of the measured flames were performed using the premixed laminar burner-stabilized flame module of ChemKin-Pro R1 2020 [57] including thermal diffusion and a multi-transport approach. With respect to the model examination process, *i.e.*, for the simulation of ST, RCM, and PFR literature data, ChemKin-Pro R1 2020 [57] was also used with the modeling approaches described in the respective publications. To tentatively assess the HCCI engine-based polygeneration process with DME or DMM as additive to CH_4, the PolyMech2.1 was further used in the engine simulations. In the following, we will describe relevant details of model development and validation (Section 3.1) as well as on the simulation of the polygeneration test cases (Section 3.2).

3.1. Kinetic model and validation

The PolyMech2.1 model extends the previous PolyMech model on fuel-rich oxidation of CH_4/DME mixtures that was developed by Porras et al. [28] and modified (to PolyMech2.0) by Kaczmarek et al. [9]. The DMM sub-mechanism is included from the recent Jacobs model [44] that was validated against a huge dataset comprising IDTs, laminar burning velocities, and speciation data at engine-relevant conditions. Their DMM sub-mechanism was developed by analogies with diethyl ether and *n*-pentane together with reaction rate

coefficients of the DMM mechanisms proposed by He et al. [58] and Vermeire et al. [59]. In addition, the PolyMech2.1 is improved by adding missing reactions of methyl formate, also taken from Jacobs et al. [44]. The added reactions lead to a better prediction of oxygenated species such as methanol and formaldehyde and other major intermediates. Finally, reaction rate coefficients of some relevant reactions are modified to improve the prediction of the flame speciation data for fuel-rich DME/CH_4 and DMM/CH_4 mixtures, as summarized in Table 2. Since the model is intended to simulate conditions covering a wide pressure range from 0.04 to 100 bar, special attention is paid to the pressure dependences of important reactions in the model development. Relevant reactions are identified by sensitivity analyses with respect to species that are not well predicted by the previous model, in particular C_2H_2, CH_2CO, and some C_3 intermediates, for several flame conditions. The sensitivity analyses can be found in Section S-II in SM2.

For these modifications, the NUIGMech1.1 [60], one of the most recent and comprehensive reaction mechanisms for C_0-C_7 species, is used as a source for the most recent thermodynamic data and reaction rate coefficients for the identified relevant reactions. Additionally, we reviewed the literature for the origin of each coefficient and possible new developments. Especially with respect to the rate coefficients of the reactions R6 and R9 in Table 2, new contributions can be found in [61] and [62], respectively. Vichietti et al. [61] proposed a new rate coefficient for the decomposition of formyl radical to CO and H radicals (R6) obtained by high-level quantum chemical methods. Nevertheless, their proposed expression is at the high-pressure limit, estimated to be at $9.8 \cdot 10^4$ atm at 700 K. In contrast, the rate coefficient proposed by Li et al. [63], also implemented in the NUIGMech1.1, represents the low-pressure limit; they showed, however, that deviations from experimentally obtained low-pressure limit data (up to 100 bar) only become significant at $T < 580$ K. Thus, the low-pressure limit rate coefficient of [63] is used in PolyMech2.1. Xu et al. [62] proposed a new theoretically-derived total rate coefficient for the CH_3 + O reaction including the branching ratios of individual products at temperatures between 200 and 2600 K. Comparing the rates obtained by this rate coefficient with those obtained by the rate coefficient of Harding et al. [64] that is implemented in the NUIGMech1.1, deviations of up to 20% at $T < 500$ K are found with an intersection at 500 K and lower deviations at higher temperatures. However, two different rate coefficients for the temperature ranges 200-1000 K and 1000-2600 K were given by Xu et al. [62], which cannot be easily implemented in the reaction mechanism. In contrast, Harding et al. [64] proposed a single rate coefficient which showed to well reproduce experimental data in the range 200-2500 K so that it is used in the present PolyMech2.1 model.

Comparing the rates of R9 and the rates obtained by the second product channel of CH_3 + O towards CO, H, and H_2, also included in PolyMech2.0 [9], the branching ratio of 0.6:0.4 (R9: Second channel) proposed by several authors [62, 65, 66] is also obtained at nearly all temperatures. Unlike in the NUIGMech1.1, in which the rate coefficient of R1 proposed by Tranter et al. [67] was reduced by a factor of 2.2, the original rate coefficient is used in PolyMech2.1.

As a further consideration, the rate constants of R2, R5, R10, and R11, R12 that were implemented independent of pressure in the previous PolyMech2.0 [9] are now described in PLOG and Troe format in PolyMech2.1, respectively, in this work. Particularly the rate of the reaction of methyl and hydroxyl radicals (R5) yielding hydrogen and formaldehyde, which can be an important product species in polygeneration processes, changes significantly at temperatures below 1000 K with increasing pressure.

Table 2. Modified reactions in PolyMech2.1 in comparison to the previous PolyMech2.0 [9] (added reactions related to methyl formate and the DMM sub-mechanism are not listed here). The reaction rate coefficients are in the form $k = AT^n\exp(-E_A/(RT))$. Units are mol, cm, s, and kJ.

Reaction		A	n	E_A	Ref.
R1	$CH_3OCH_3 + CH_3 = CH_3OCH_2 + CH_4$	$1.019\cdot10^{1}$	3.78	40.560	[67]
R2	$C_2H_3 + O_2 = CH_2CHO + O$	$1.600\cdot10^{23}$	-3.22	36.388	[68][a,b]
R2	$C_2H_3 + O_2 = CH_2CHO + O$	$6.670\cdot10^{9}$	0.72	3.256	[68][a,b]
R3	$C_2H_2 + O = HCCO + H$	$2.958\cdot10^{9}$	1.28	10.343	[69]
R4	$C_2H_2 + O = CH_2 + CO$	$7.395\cdot10^{8}$	1.28	10.343	[69]
R5	$CH_3 + OH = CH_2O + H_2$	$5.374\cdot10^{9}$	0.29	1.172	[70][b]
R6	$CHO + M = CO + H + M$	$4.749\cdot10^{11}$	0.66	62.216	[63]
R7	$C_3H_8 (+M) = C_2H_5 + CH_3 (+M)$	$1.550\cdot10^{24}$	-2.03	378.183	[71][c]
R8	$CH_3OCH_3 (+M) = CH_3 + CH_3O (+M)$	$2.330\cdot10^{19}$	-0.66	352.04	[72][c]
R9	$CH_3 + O = CH_2O + H$	$5.540\cdot10^{13}$	0.05	-0.570	[64]
R10	$C_3H_3 + C_3H_3 = C_6H_6$	$3.889\cdot10^{50}$	-11.01	85.019	[73][b]
R11	$HOCHO (+M) = CO + H_2O (+M)$	$7.500\cdot10^{14}$	0.00	287.483	[74][c]
R12	$HOCHO (+M) = CO_2 + H_2 (+M)$	$4.500\cdot10^{13}$	0.00	285.516	[74][c]

[a] The rate coefficient of R2 was fitted by a sum of two modified Arrhenius equations.
[b] At p=10 bar. See SM3 for rate coefficients at different pressures.
[c] See SM3 for low-pressure limits and Troe parameters.

The final PolyMech2.1 kinetic model consists of 947 reactions and 192 species and has the advantage of being much smaller than other typical DME/DMM/CH_4 models, *e.g.*, the models of Jacobs et al. [44] (2889 reactions, 530 species) and Sun et al. [75] (2824 reactions, 524 species). It therefore allows for a significantly reduced computational cost for engine simulations (see Section 4.2), while still permitting to predict the

formation of key soot precursors such as benzene and some larger PAHs such as pyrene. An appropriate estimate of the extent of soot precursor formation is of particular importance for the identification of suitable engine conditions for polygeneration processes that typically operate under fuel-rich conditions. Note that the low-temperature chemistry and the involved important oxygenated species such as the ketohydroperoxide ($HOOCH_2OCHO$) are also included in the mechanism. The PolyMech2.1 model developed here is thus expected to be a well-suited prediction tool for an engine-based polygeneration process.

For a critical inspection, the PolyMech2.1 model was first examined against the measured flame data in this study (see Section 4.1 for details). Furthermore, Section S-III in SM2 includes a comparison with the recently validated Jacobs model [44], showing that the PolyMech2.1 model can consistently and satisfactorily reproduce the flame data for major species and most of the intermediate species under different conditions, with a quality quite similar to the predictions of the Jacobs model [44]. In addition, experimental data from the literature at elevated pressure and $\Phi \geq 2$ were selected for model inspection to assess its performance for engine-like and polygeneration-relevant conditions. In particular, data obtained with DME/CH_4 mixtures in different facilities were used, including speciation in a ST [9] and PFR [9, 26, 28], and IDTs in a ST and RCM [22]. With respect to DMM/CH_4 mixtures, only limited data are available in the literature and we examined the IDT measurements in a ST by Herzler et al. [14]. The inspected experimental dataset thus covers equivalence ratios of 2-20, temperatures of 400-2000 K, and pressures of 0.04-100 bar. The comparisons between model predictions and experimental data are included in Section S-IV in SM2, and only selected results are presented here: Speciation data of DME/CH_4 in a PFR at high equivalence ratios and intermediate to high pressures in Fig. 2; IDT data of DME/CH_4 and DMM/CH_4 in a ST and an RCM at intermediate to high equivalence ratios and pressures in Fig. 3. As can be seen here and in SM2, overall respectable agreement is shown with capturing the trends consistently and matching quantitative results within the experimental uncertainties in most cases. The large deviation in the absolute mole fraction of CH_2O in the high-pressure case (Fig. $2c_2$) might be related to the low signal-to-noise ratio in the experiments, as mentioned in the respective paper [26] , that could lead to higher uncertainties than the assumed 20%. The IDTs for the 5% DMM mixture at Φ=10 are also noted to be overpredicted at temperatures higher than 1050 K (Fig. 3a). However, this result is not surprising, since the deviation was also found for several reaction mechanisms in the original paper [14], including that of Jacobs et al. [44].

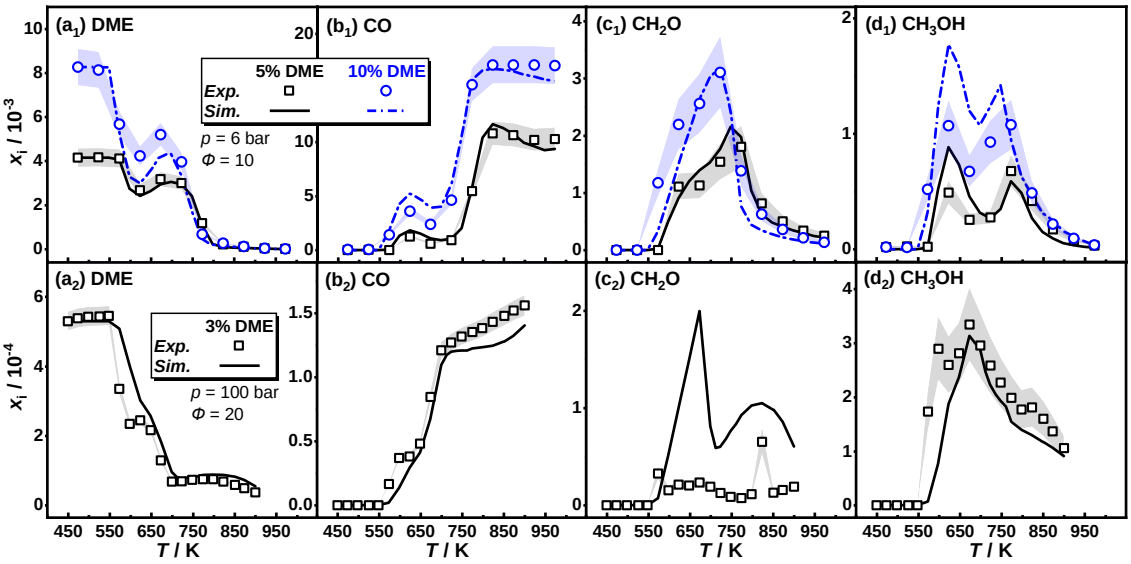

Fig. 2. Comparison of PolyMech2.1 model results with the experimental DME/CH_4 PFR speciation data of Porras et al. (upper figures: p=6 bar, Φ=10) [28] and Hashemi et al. (lower figures: p=100 bar, Φ=20) [26].

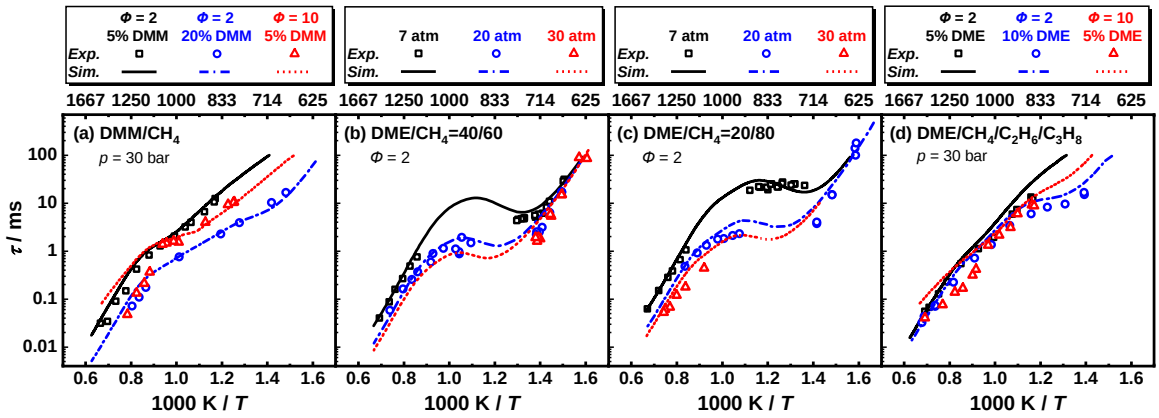

Fig. 3. Comparison of PolyMech2.1 model results with the experimental IDT data of DMM/CH_4 in ST from Herzler et al. ((a): p=30 bar, Φ=2, 10) [14], DME/CH_4 in ST and RCM from Burke et al. ((b, c): p=7, 20, 30 atm, Φ=2) [22], and DME/CH_4/C_2H_6/C_3H_8 in ST from Kaczmarek et al. ((d): p=30 bar, Φ=2, 10) [9].

3.2. Polygeneration test cases

To examine polygeneration-relevant conditions regarding the potential feasibility of DME and DMM as performance-enhancing additives, we have performed selected engine simulations with the validated PolyMech2.1 model. In these simulations, several typical HCCI engine configurations were selected, and yields of syngas, together with work and heat, were analyzed with respect to exergetic and kinetic aspects for conditions of relevance, varying mainly size (bore/stroke ratio), rotation speed, and inlet temperatures. These simulations are thought to provide some insight into the influence of important parameters and may guide respective experiments in different existing engine environments.

The HCCI engine was represented by a time-dependent four-stroke single-zone model with detailed chemical kinetics and was modeled in Cantera [76] within Python. In this framework, a homogeneous reactor model with a time-varying volume was used. The piston velocity was calculated according to [77]. For each time step, the cylinder volume was calculated, and energy and species conservation equations were solved using an ODE solver, depending on the respective stroke, assuming a closed system during inlet valve closing (IVC) and exhaust valve opening (EVO) and an open system between EVO and IVC. The differential equations were described in our previous work [78]. The general maximum time step is 10^{-5} s, however, each time step can be additionally subdivided to prevent convergence issues. An ideal gas behavior was assumed for the cylinder charge. The mass flows through the inlet and outlet valves depend on the pressure difference to their fresh gas and exhaust gas environment. While the fresh gas environment is at ambient pressure, the exhaust back pressure is assumed to be 0.2 bar. The species generation is based on the elementary reaction mechanism developed in this study.

The convective heat transfer through the cylinder walls was calculated using the literature heat transfer model from Chang et al. [79] according to Eq. (4):

$$h\,(t) = C \cdot L(t)^{-0.2} \cdot p(t)^{0.8} \cdot T(t)^{-0.73} \cdot (C_1 \cdot \overline{s}_p + C_2/6 \cdot V_d/V_r \cdot T_r/p_r \cdot (p(t) - p_{mot}(t)))^{0.8} \quad (4)$$

where C, C_1, and C_2 are constants taken from [79] (C=110, C_1=6.18, and C_2=0 during gas exchange stroke, C_1=2.28 and C_2=0 during compression and expansion, and C_1=2.28 and C_2=$3.23 \cdot 10^{-3}$ m/(s·K) during combustion), V_d is the displacement volume, L is the actual cylinder height, p, p_{mot}, and T are the actual in-cylinder pressure, motored pressure, and temperature, respectively. V_r, T_r, and p_r are reference conditions, usually chosen at IVC, and $\overline{s}_p$ is the mean piston speed. This heat transfer model is chosen here since it is designed for the prediction of heat losses in HCCI engines.

The chosen modeling approach has been shown to be feasible in terms of the species prediction in previous polygeneration studies [2]. In addition, a comparison between the single-zone model (SZM) and a multi-zone model (MZM) with 12 zones [80] of an HCCI engine performed by Freund et al. [81] showed that the number of zones has no significant effect on the fuel conversion, species production, and exergetic efficiency. Since the simulation time increases strongly with the number of zones, the SZM was used in this feasibility study to save computational time. It should be mentioned that, as a compact model, PolyMech2.1 showed the advantage of significantly decreased simulation times (by a factor of 20 (SZM) to 300 (12 zone MZM))

compared to the recent Jacobs model [44]. This allows to perform systematical parameter studies and utilize optimization procedures with acceptable computational cost. For the entire parameter study carried out here, the computation time was 137 hours using 16 CPU cores.

We have chosen three generic engine types for these simulations (oriented towards, *e.g.*, car engines or ship engines) which mainly differ in size (bore (in mm)/stroke (in mm): 81/95.5-460/580) and speed (600-3000 min^{-1}) to identify potentially advantageous operation conditions for the discussed polygeneration process. DME/CH_4 and DMM/CH_4 mixtures with air as the oxidant were analyzed for intake temperatures (T_0) of 323-723 K, equivalence ratios of 1-10, and additive amounts of 0%-20% with a specific focus on syngas production. To enable the ignition of the CH_4/air mixture, the necessary intake temperatures and the required amount of additive were determined. A brief summary of the chosen engine parameters and operation conditions can be found in Section S-VI in SM2.

4. Results and discussion

In the following sections, the flame results will be discussed first (Section 4.1) in terms of the major species behavior (Section 4.1.1) and fuel-specific intermediate species formation (Section 4.1.2). Special attention will be paid to the yields of interesting products under different conditions, *e.g.*, syngas, selected hydrocarbons, and oxygenated compounds. Subsequently, the validated PolyMech2.1 will be used to explore potentially favorable polygeneration conditions using DME/CH_4 and DMM/CH_4 mixtures in the assumed HCCI engine environments (Section 4.2). These explorative parameter studies will focus on the formation of syngas, together with work and heat output, as well as sooting propensity and exergy analyses.

4.1. Flame results and related discussion

4.1.1. Major species behavior and syngas yields

Experimental mole fraction profiles of the fuels (DME, DMM, CH_4) and yield profiles of the produced syngas (CO, H_2) are given in Fig. 4, together with the model predictions. Speciation data of other major species (O_2, H_2O, CO_2) for the DME- and DMM-related flame series are provided in Section S-V in SM2.

As can be observed, the flame structure in different flames can be consistently and satisfactorily reproduced by the PolyMech2.1 model, indicating that the model can properly describe the underlying flame chemistry. A shift of the flame front downstream upon a partial replacement of DME or DMM by CH_4 at the same Φ of

1.7 can be noted from the fuel consumption profiles in Fig. 4a_1,a_2 indicating a decreasing burning velocity that is in line with literature results for DME/CH_4 mixtures [19, 21, 25, 27, 31]. Also, both DME and DMM exhibit a more rapid consumption than CH_4 along the height above the burner, suggesting a higher reactivity of the $OME_{0\text{-}1}$ fuels compared to CH_4, underlining their suitability as ignition enhancers in the discussed polygeneration process. Note that an enhanced stability of CH_4 flames with DME addition was already previously confirmed [31].

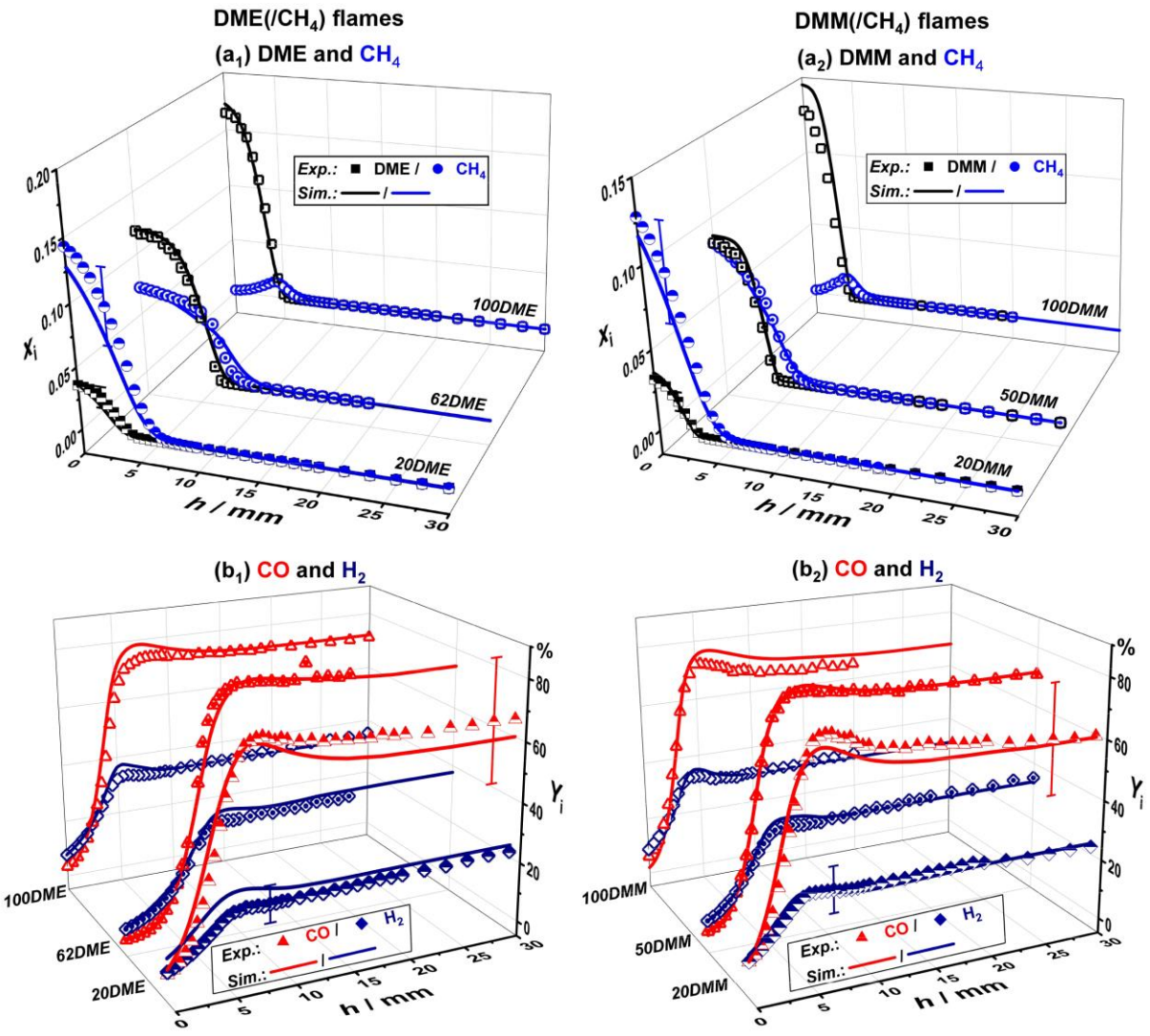

Fig. 4. Mole fraction profiles of the fuels (a_1,a_2) and yield profiles of H_2 and CO (b_1,b_2) for the investigated DME (/CH_4) (left) and DMM (/CH_4) (right) flames. Symbols: Experimental results; Lines: PolyMech2.1 model results. Error bars are given for selected points to show the experimental uncertainty.

Rate of production (ROP) analyses of the investigated flames were performed in order to understand the reaction patterns of the different fuel mixtures at different Φ, as shown schematically in Fig. 5. H-abstraction

reactions (majorly by H and OH etc.) dominate the consumption pathways of both DME and DMM with contributions of over 75% for the DME(/CH_4) and 38% for the DMM(/CH_4) flames, forming the fuel radical(s) CH_3OCH_2, and $CH_3OCHOCH_3$ and $CH_3OCH_2OCH_2$, respectively. Similarly, CH_4 is mostly converted into CH_3 radicals. Partial replacement of DME or DMM by CH_4 at the same Φ of 1.7 has only minor influence on the main consumption pathways, in agreement with previous flame studies on DME/*iso*-butane [82], DME/*n*-heptane [83], DME/*iso*-octane [84], and DMM/ethane [40]. As seen from the ROP analyses in Fig. 5, the contributions of the respective routes to DME, DMM, or CH_4 consumption are only slightly changed upon the partial replacement of DME or DMM by CH_4 at Φ = 1.7. This is not surprising, since the reaction patterns in Fig. 5 reveal that the interactions between CH_4 and DME or DMM are majorly limited to the interconversion of CH_4 and CH_3. Nevertheless, the mole fraction of species might differ in different flames due to the differences in the C/H/O ratio and temperature profile. In addition, unimolecular decomposition reactions also contribute considerably to the consumption of both DME (*via* $CH_3OCH_3 = CH_3O + CH_3$) and DMM (*via* $CH_3OCH_2OCH_3 = CH_3OH + CH_3 + CHO$ and $CH_3OCH_2OCH_3 = CH_3OCH_3 + CH_2O$), especially at Φ=1.7. The C–O bond scission of DME produces CH_3 and CH_3O, whereas DMM can undergo at least two bond scission paths to form intermediates such as CH_3OCH_3 (DME) and CH_2O (formaldehyde), and CH_3OH (methanol), respectively.

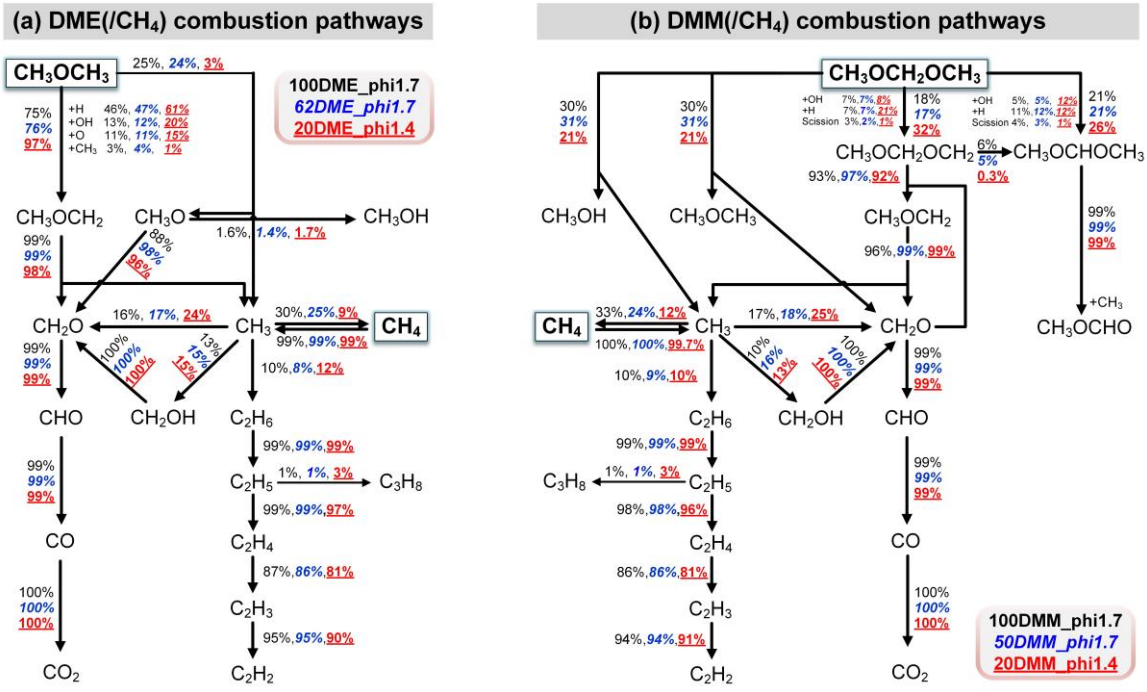

Fig. 5. Main reaction networks of the investigated DME (/CH_4) (a) and DMM (/CH_4) flames (b) based on the ROP analyses by integrating the ROP coefficients along the entire flame range using the PolyMech2.1 model. The numbers are percent contributions to the consumption of the species on the source side of the arrow.

Not unexpectedly, the equivalence ratio noticeably affects the importance of different consumption pathways. At lower Φ, the unimolecular decomposition routes become less important for both DME and DMM consumption, while the H-abstractions show higher contributions primarily due to the increased concentrations of OH and O.

Interestingly, in the studied flames, relatively clean syngas can be formed as stable product in the burnt gas with relatively high yields of up to ~78% for CO and ~35% for H_2 depending on the conditions, pointing towards potentially efficient syngas production in a polygeneration process. As shown in Fig. 4, the addition of CH_4 into a DME or a DMM flame at Φ=1.7 slightly enhances the yields of both, CO and, less pronouncedly, of H_2, *e.g.*, from ~65% and ~32% for 100DMM to ~72% and ~35% for 50DMM/50CH_4, respectively. However, this behavior does not necessarily apply to polygeneration-relevant conditions. For instance, as will be presented later in Section 4.2, a higher CH_4 fraction of the DME/CH_4 mixtures in the model engine could also reduce the syngas yield at a Φ of ~3.0. Obviously, most of the consumed carbon in the flame is finally converted into CO, primarily *via* the typical combustion pathways of $CH_2O \rightarrow CHO \rightarrow CO$, where CH_2O is majorly formed from the fuel fragments (*e.g.*, CH_3OCH_2, CH_3O, CH_3) or directly from the bond scission of DMM (see Fig. 5). As seen from Fig. 4b_1,b_2, DME exhibits a slightly higher syngas yield (especially H_2) in comparison to DMM, in line with the engine simulation results discussed later in Section 4.2. As expected, the yield of CO and more pronouncedly that of H_2 decreases slightly towards Φ=1.4 due to the enhanced oxidizing conditions, confirming that a richer condition might be favored for syngas production in a polygeneration process using the DME/DMM/CH_4 fuel system. Similarly, the above results indicate a more pronounced effect of the equivalence ratio than of the DME or DMM additive amount.

4.1.2. Intermediate species formation

Apart from CH_4, numerous C_1-C_4 hydrocarbon and oxygenated intermediates were detected in all investigated flames. The combination of CH_4 with DME or DMM does not result in the formation of new intermediates but alters noticeably most of their concentrations. The discussion here focuses on experimental and simulated mole fractions of several products that are potentially interesting for a polygeneration process, *i.e.*, C_2H_2 (acetylene), C_2H_4 (ethylene), and C_2H_6 (ethane) in Fig. 6, as well as CH_2O (formaldehyde), CH_3OH (methanol), and CH_3OCHO (methyl formate) in Fig. 7. Note that the detection of $C_2H_4O_2$ was typically not reported in previous MBMS studies of premixed DME flames [37-39, 83-85], which might be due to overlapping signals with the neighboring C_3H_8O peak. Here, $C_2H_4O_2$ is calibrated as CH_3OCHO for all

investigated flames, since it is one of the major intermediates in low- to intermediate-temperature DME oxidation [86] and was already detected previously in premixed DMM flames [40, 87]. Moreover, to better visualize the formation tendency of these species under different conditions, their maximum yields along the height above the burner are given in the insets of Fig. 6 and Fig. 7.

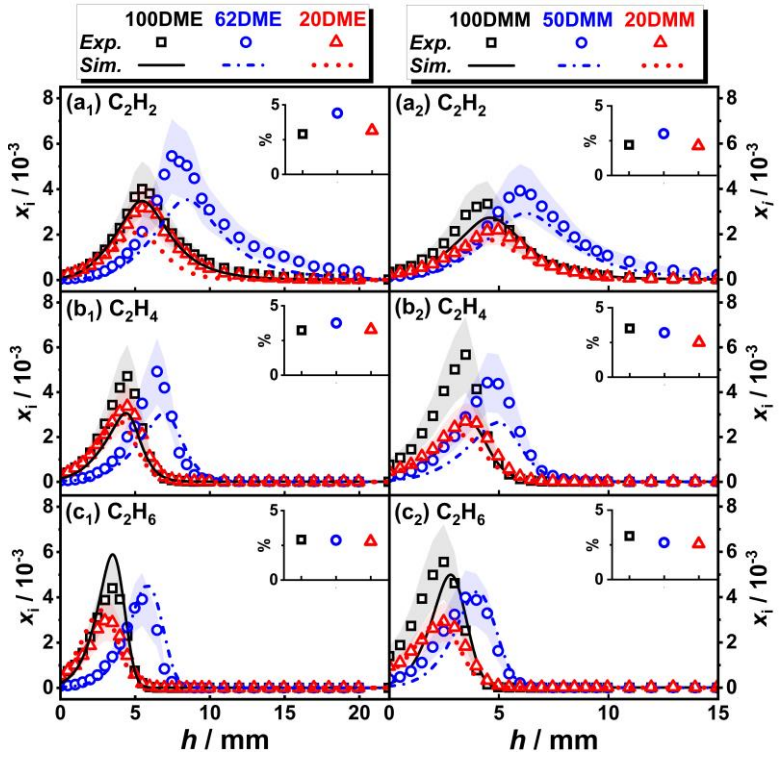

Fig. 6. Mole fraction profiles of C_2H_2 (a), C_2H_4 (b), and C_2H_6 (c) for the investigated DME(/CH_4) (left) and DMM(/CH_4) (right) flames. The maximum experimental yield of each species in different flames is given in the insets.

Several other intermediates were also detected in all investigated flames, but with mostly lower mole fractions. These species are beyond the focus of the discussed polygeneration process, but their detailed speciation data and discussions are beneficial for the understanding of the fundamental kinetics and are therefore presented in Section S-V in SM2, including C_3H_4 (calibrated as propyne), C_3H_6 (propene), C_3H_8 (propane), C_4H_6 (calibrated as 1,3-butadiene), CH_2CO (ketene), CH_3CHO (acetaldehyde), $CH_3OC_2H_5$ (methoxyethane), and the two radicals CH_3 (methyl) and C_3H_3 (propargyl) for both the DME and DMM flame series, as well as C_2H_6O (calibrated as DME, although some presence of its isomer ethanol may not be ruled out [88]) and an unspecified species $C_4H_9O_2$ that were additionally detected as intermediates in the DMM flames. Assignment of these species are consistent with previous measurements and/or pertinent

modeling studies on DME and DMM flames [37-40, 83-85, 87, 89, 90]. Note that most of these species are not easily accessible in PFR, ST, and RCM conditions [9, 23, 26, 28].

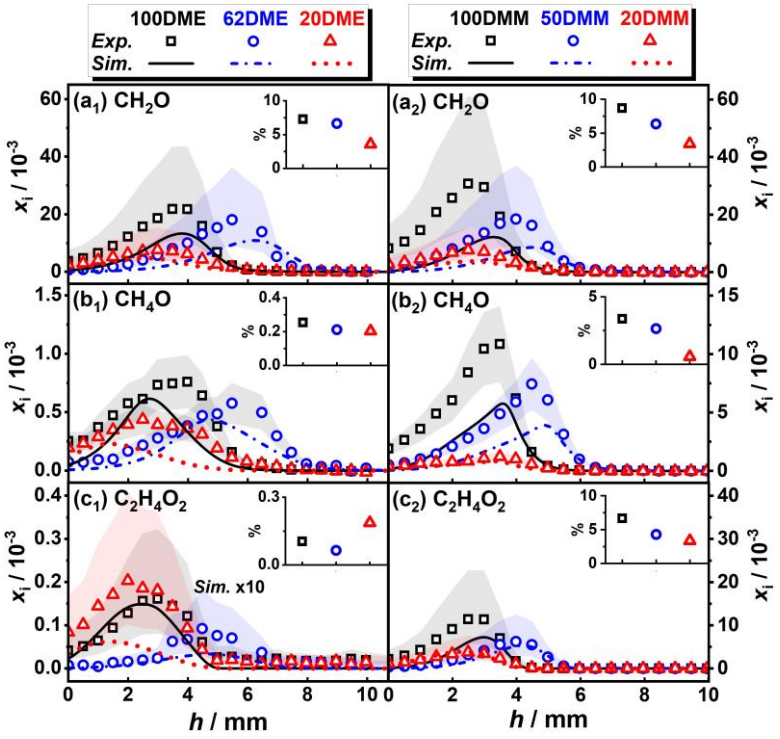

Fig. 7. Mole fraction profiles of CH_2O (a), CH_4O, calibrated as CH_3OH (b), and $C_2H_4O_2$, calibrated as CH_3OCHO (c) for the investigated DME(/CH_4) (left) and DMM(/CH_4) (right) flames. The maximum experimental yield of each species in different flames is given in the insets.

As shown in Fig. 6, C_2H_2, C_2H_4, and C_2H_6 are the major hydrocarbon intermediates for all investigated flames with maximum mole fractions of up to 10^{-3} and yields of 2.1%-4.4%. Due to the absence of a C–C bond in the DME or DMM molecule, the intermediately formed CH_3 radical dominates the production of these C_2 hydrocarbons through an initial recombination and the subsequent dehydrogenation processes: $CH_3 \rightarrow C_2H_6 \rightarrow C_2H_5 \rightarrow C_2H_4 \rightarrow C_2H_3 \rightarrow C_2H_2$ (see Fig. 5). This mechanism accounts for the observed earlier build-up of C_2H_6 than of C_2H_4 and C_2H_2 in Fig. 6. As seen from the figures in Section S-V and Fig. 6, upon combination of DME or DMM with CH_4, the yields of CH_3 and its recombination product C_2H_6 are not perceptibly enhanced, and even, surprisingly, slightly decreased in the DMM flames, indicating that in comparison to CH_4 fuel, a net formation of CH_3 is comparably favored in the DME or even more favored in the DMM flame. Nevertheless, combining CH_4 with DME or DMM at the same Φ leads to a slight increase of C_2H_2 yield in both series of flames (see Fig. $6a_1$,a_2).

CH_2O is the dominant oxygenated intermediate in all investigated flames with maximum yields of up to 7.3%

and 8.7%, respectively, in the 100DME and 100DMM flames, as seen in Fig. 7. Interestingly, CH_3OH and CH_3OCHO also show comparably high mole fractions of up to 10^{-3}-10^{-2} and yields in the range of 0.6%-6.7% in the DMM(/CH_4) flames, which is 1-2 orders of magnitude higher than those observed in the DME(/CH_4) flames. The ROP analyses for DMM(/CH_4) flames suggest that unimolecular decompositions of the fuel and the major fuel radical $CH_3OCHOCH_3$ provide additional fuel-specific routes that are even predominant for CH_3OH and CH_3OCHO formation with contributions of over 96% in all DMM (/CH_4) flames. This behavior suggests DMM as a potentially interesting fuel additive for a polygeneration process that targets production of high-value chemicals (*e.g.*, formaldehyde, methanol, methyl formate) [2, 28, 91]. Nevertheless, this statement should be regarded with caution, since OME_n fuels are commonly produced from a multi-step synthesis involving methanol and formaldehyde [91, 92]. Due to the presence of C–O bonds in the molecule, DME and DMM are expected to feature a higher formation propensity of oxygenated compounds than hydrocarbons [23, 40], in line with the observations in Fig. 7 that combining CH_4 with DME or DMM in flames at the same Φ slightly decreases the yields of all presented oxygenated intermediates. Moreover, a lower Φ of 1.4 in combination with a higher CH_4 fraction further decreases the yields of these species, partially due to a favored formation of the fully oxidized product CO_2. However, an exception occurs for CH_3OCHO in the 20DMM/80CH_4 flame, where an enhanced yield is observed at Φ=1.4 (see Fig. 7c_1). The model prediction cannot capture this behavior and also remarkably under-estimates the CH_3OCHO mole fractions for all DME (/CH_4) flames, suggesting that uncertainty exists in the experiments or model for CH_3OCHO. The ROP and sensitivity analyses at the position of the maximum mole fraction of CH_3OCHO showed that DME → CH_3OCH_2 → $CH_3OCH_2O_2$ → CH_3OCH_2O → CH_3OCHO is the main formation pathway of CH_3OCHO, while the reactions $CH_3OCH_3 + H = CH_3OCH_2 + H_2$ and $CHO = H + CO$ are the most sensitive to the CH_3OCHO mole fraction. Thus, these reactions, and possibly missing reactions to form CH_3OCHO might need to be revisited in future studies.

4.2. Model-assisted exploration of a polygeneration process for the selected HCCI engine test cases

Polygeneration outputs of interest from HCCI engines include syngas, work, and heat. Here, we focus on achieving maximum yields of syngas at favorable H_2/CO ratios without using excessively high intake temperature for DME and DMM as ignition enhancing additives to methane which also serve to control the combustion phasing. As a first step, reasonable operating conditions were tested systematically. Since this parameter variation is only intended to select conditions for an assumed polygeneration process, we will limit

the description to some major aspects of importance for the further discussion (for details see Section S-VI in SM2).

The necessary intake temperature T_0 and additive amounts to achieve a stable combustion phasing of 5° before top dead center (bTDC) to 10° after top dead center (aTDC) were determined and reasonable operating conditions were tested. To this end, T_0 was varied between 323 K and 723 K for additive amounts of DME or DMM between 0% and 20% at Φ=2.5, assuming an engine with a bore/stroke ratio of d/s=460 mm/ 580 mm and a rotation speed of N=600 min^{-1}. For neat CH_4/air mixtures, T_0 >423 K is necessary to avoid misfires and addition of work to the system. Below 423 K, the CH_4 conversion and syngas yield are insignificant with <5%. Above T_0 >423 K, CH_4 conversion and syngas yield increase rapidly to >80% and >60%, respectively, while the provided work has a maximum at 573 K associated with optimal combustion phasing. Higher temperatures can lead to premature ignition and possibly knocking. As expected, the addition of DME and DMM to CH_4 has a reactivity-enhancing effect under the selected engine conditions and leads to an (earlier) ignition even at low temperatures. The main effect of DME or DMM addition is the formation of radicals at lower temperatures so that the consumption of methane is initiated earlier compared to neat CH_4 mixtures. The formation of CH_3 radicals is also slightly enhanced and the pathways towards formaldehyde are slightly preferred instead over the formation of higher hydrocarbons such as ethane (similar as the behavior in flames shown in Fig. 5). Nevertheless, the range of operation is limited for both additives: A DME amount of 2%-5% is required, while more DME leads to an unstable combustion phasing because of premature ignition. In contrast, an additive amount of 3%-8% DMM is required while higher amounts lead to a reduced reactivity due to the larger heat capacity. The larger heat capacity reduces the temperature after compression with increasing DMM amount and prevents ignition. Hence, the effect of lower intake temperatures cannot be compensated by a higher amount of DMM due to the higher specific heat capacity and the higher mass fraction of DMM at the same molar additive amount. Further tests indicated that a higher Φ shifts this phenomenon towards higher temperatures and higher additive amounts.

For a comparison of the additives with respect to the production of syngas as well as work and heat output for several conditions, we describe some of the needed parameters for this analysis first and have then applied this formalism to different engine sizes. The work and heat outputs were obtained from the integral $W = -\int p\mathrm{d}V$ and from Fourier's law, respectively. The yields of H_2 and CO were computed according to Eq. (3) and the syngas yield as a whole was determined by $Y_{H2} \cdot Y_{CO}$. Additionally, the combustion phasing

was analyzed by calculating the released heat per time unit according to Eq. (5):

$$\dot{Q}_{HR} = V(t) \cdot R \cdot T(t) \cdot \sum_i (h_i^0 \cdot \dot{\omega}_i) \quad (5)$$

Here, R is the ideal gas constant, h^0 is the nondimensional standard molar enthalpy of formation at the current temperature and pressure, and $\dot{\omega}$ is the net production rate (kmol·m^{-3}·s^{-1}). The index i is related to each species that is present at this time step. To evaluate the combustion phasing, the crank angle at which 50% of the heat has been released (CA_{50}) was determined.

For the following discussion, we focus primarily on the engine with the parameters given above which is oriented to a ship-size engine, while additional information on the other test cases is available in Section S-VI in SM2. A comparison of the outputs as a function of equivalence ratio and additive amount for T_0=423 K using DME or DMM as additive is depicted in Fig. 8, in terms of the syngas yield, H_2/CO ratio, as well as power and heat output. The conversion of the respective fuels and the further products are not depicted here.

ROP analyses in the engine simulations showed that the global pathways for the consumption of DMM, DME, and CH_4, and the formation of the end products is similar under engine conditions to those in the flame conditions (see the ROP analyses for flames in Fig. 5). Only with respect to DMM, the engine conditions feature the formation of more unstable low-temperature intermediates such as $CH_3OCH_2OCH_2O$ due to the relatively low temperature.

As shown in Fig. 8a$_1$, the syngas yield can reach up to 77% while CH_4 conversion reaches 99% for Φ=3 and a DME amount of 18%. The model predicts that with further decreasing Φ, *i.e.*, below 2, the product gas composition consists increasingly of CO_2 and H_2O, while Φ >3 leads to an increased formation of higher hydrocarbons including C_2H_2 ($Y_{C2H2} \approx 1\%$), C_2H_4 ($Y_{C2H4} \approx 9\%$), and C_6H_6 ($Y_{C6H6} \approx 3\%$), and PAHs such as naphthalene and pyrene.

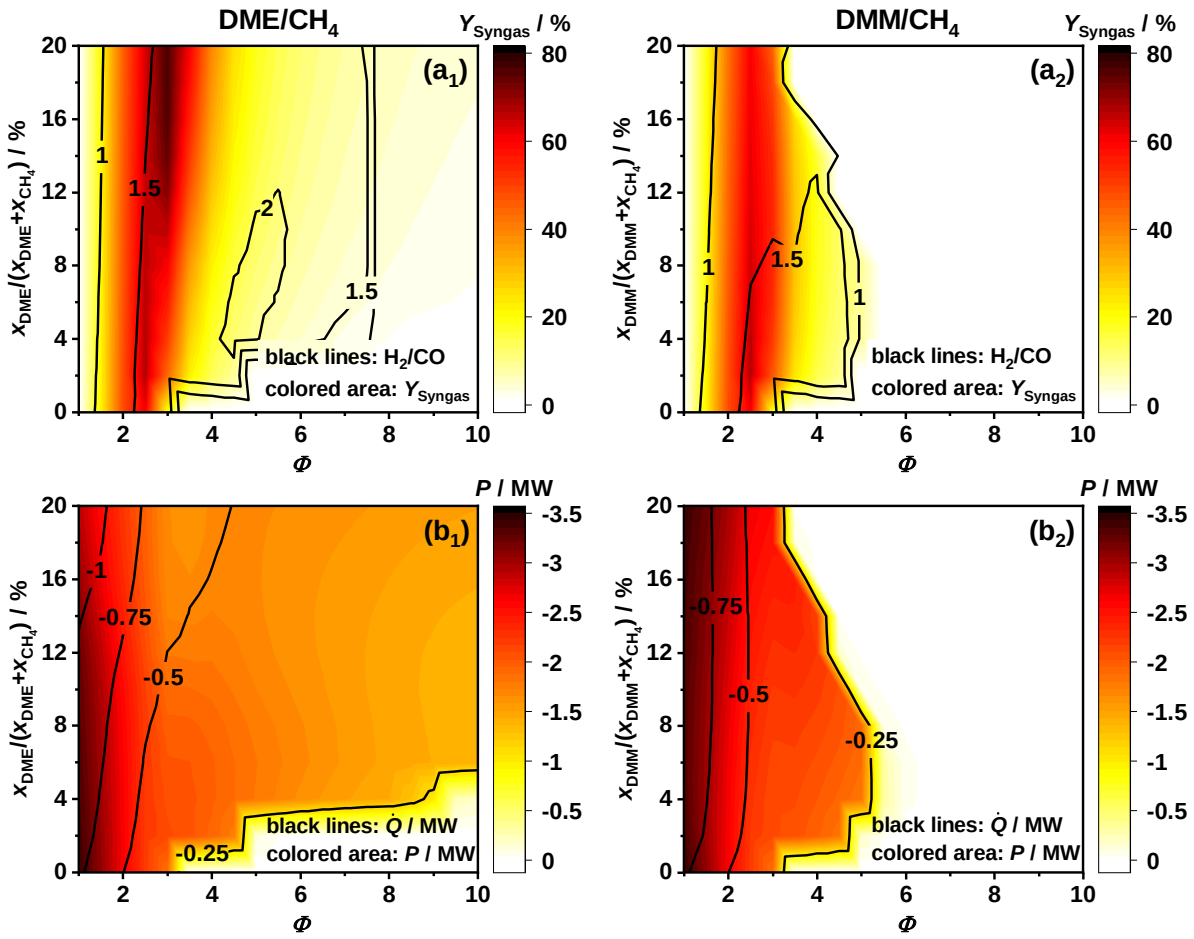

Fig. 8. Syngas yields, H_2/CO ratios, and heat ($\dot{Q}$) and work (P) outputs as a function of the additive amount $x_{ad}/(x_{ad}+x_{CH4})$ and the equivalence ratio for DME/CH_4 mixtures (a_1,b_1) and DMM/CH_4 mixtures (a_2,b_2). The engine parameters/conditions are: T_0=423 K, d/s =460 mm/ 580 mm, N=600 min^{-1}. Note that according to thermodynamic conventions, P and $\dot{Q}$ carry a negative sign when transferred from the system.

Furthermore, modeling results show that CH_4 conversion decreases to 20% with increasing Φ whereas DME is then still completely converted. For a range of equivalence ratios of 2.5-3, a DME amount of 2%-5% is reasonable with respect to the combustion phasing and power and heat output as shown in Fig. $8b_1$; however, higher Φ requires higher DME amounts for a respective maximum power and heat output. At the aforementioned conditions (Φ: 2.5-3, 2-5% DME), a syngas yield of ~67% could be achieved while CH_4 and DME are completely converted. These results are competitive with those of previous studies [7, 12], in which the influence of DME on an engine-based polygeneration process was experimentally and theoretically investigated using a slow-rotating (N=600 min^{-1}) engine with a six times smaller volume-to-surface ratio than assumed here. These authors [7] report a minimum DME amount of 9% at Φ=2 to achieve stable operation, providing a CH_4 conversion of ~90% and a syngas yield of ~45% with the noted differences mainly due to the different engine sizes.

Considering DMM as an additive, the maximum syngas yield is up to 67% for a Φ of 2.5 and 3% DMM addition, as shown in Fig. 8a_2, which is slightly lower than the maximum in the DME case. In contrast to DME, DMM amounts of >14% lead to misfires which explains the decreasing syngas yields and the positive sign in the power output with increasing DMM amount. With increasing Φ, the effect of the specific heat capacity is amplified: The more DMM is used, the lower is the Φ at which misfires predominate and not even the additive is converted. Taking these effects into account, the most reasonable DMM amount is between 3% and 5%. The conversions of CH_4 and DMM decrease to 10% and 40%, respectively, for Φ=6, while at Φ >6, no conversion is observed. The overall power and heat output is lower compared to DME, because of the lower heating value and higher mass fraction of DMM at the same molar additive amount, as observed in Fig. 8b_2.

The H_2/CO ratio of the obtained syngas for both DME or DMM as additives varies between 1 and 3 and depends on the equivalence ratio and fuel conversion. The obtained H_2/CO ratios are ~1 in a range of Φ of 1.5-2.5 and near 2 at an equivalence ratio of approximately 4. The H_2/CO ratios that might be obtained with both additives are seen to be attractive for the production of chemicals in different applications [93] together with heat and work with equivalence ratios of 2.5-3. Interestingly, we could also show that the use of DMM requires lower molar amounts of the additive.

Considering a possible sooting problem, the formation of PAHs such as naphthalene ($C_{10}H_8$), phenanthrene ($C_{14}H_{10}$), and pyrene ($C_{16}H_{10}$) was tentatively evaluated in the simulations in a Φ range of 2.5-7. Regarding the attractive compact size of the model, it should be kept in mind that its capability to predict soot precursor and PAH formation is limited. Nevertheless, DME generally shows a broader Φ range for PAH formation in slightly higher amounts than DMM. For instance, an addition of 5% DME could result in the formation of up to 1% $C_{16}H_{10}$ and 5% $C_{10}H_8$ in the Φ range of 4-7, while 5% DMM addition is simulated to form slightly lower amounts of 0.5% $C_{16}H_{10}$ and 4% $C_{10}H_8$ only in a very narrow Φ range near ~ 4. Additionally, it can be noted that more DME leads to an increased PAH formation while more DMM leads to a decreased PAH formation (by up to 1%) at a similar fuel and additive conversion. Up to Φ ~5, nearly no PAHs are predicted for DMM addition. This trend might be of particular interest with respect to the production of higher hydrocarbons such as acetylene, ethylene, and benzene, typically performed at such high Φ. The above results indicate that although the use of DME appears to be more advantageous with respect to syngas production, DMM could be more promising for the production of higher hydrocarbons due to its lower sooting propensity

at high Φ.

The general trends for the additive performance were also inspected for the different engine test cases mentioned in Section 3.2, ranging from the slow-rotating engine with a high volume-to-surface ratio (oriented to ship engine sizes) discussed above to a fast-rotating engine with a small volume-to-surface ratio (oriented to car engine sizes). The comparison of relevant outcomes for the different engines is shown in Section S-VI in SM2. As expected, heat losses are higher for smaller engines, leading to lower temperatures in the cylinder and to lower syngas yields. This is especially noted for the DMM/CH_4 mixtures because of the higher heat capacity of DMM compared to DME. Higher rotation speeds lead to a decreased time for the reaction and faster quenching as expected, leading to decreased syngas yields as well. Although the fast-rotating engines generally have a high flow rate, it could not compensate for the decreased syngas yields in terms of mass flow. Instead, the kinetically induced disadvantages predominate.

In addition to the evaluation of the outputs, an exergetic analysis was performed to examine exergy losses and the general feasibility of the process. The exergetic efficiency η_{ex} was calculated according to the classical thermodynamic relation shown in Eq. (6):

$$\eta_{ex} = 1 - \dot{E}_{loss} / \dot{E}_{in} \quad (6)$$

The inlet exergy $\dot{E}_{in}$ describes the sum of all specific chemical exergies in the present mixture. The specific chemical exergies are computed *via* the chemical equilibrium method, which is described in [78] ranging from 9.8 MJ/kg (CO) to 117.1 MJ/kg (H_2).

The exergy losses $\dot{E}_{loss}$ are defined *via* the irreversible entropy production $\dot{S}_{irr}$ and are calculated by Eq. (7):

$$\dot{E}_{loss} = T_u \cdot \dot{S}_{irr} = T_u \cdot \dot{m} \cdot (s_1 - s_0) - \dot{Q}/T_u \quad (7)$$

Here, T_u is the ambient temperature, m is the mass of the cylinder charge, s_1 and s_0 are the specific entropies at time step zero and the end of the cycle, and $\dot{Q}$ is the heat transfer to the wall determined *via* Fourier's law as described above.

Figure 7a shows the power and heat flow, the in- and outflowing exergies, the outflowing chemical exergy of H_2, and the exergetic efficiency for an additive amount of 5% and an intake temperature of 423 K derived from the slow-rotating engine with a high volume-to-surface ratio. In general, the inflowing chemical exergy is higher than the outflowing chemical exergy because the chemical exergy of the products, especially of CO,

CO_2, H_2O, and N-containing species is lower than the chemical exergy of the fuel and the additive. The in- and outflowing exergies increase with increasing Φ due to the increasing fuel and additive amount. The contradiction that the total outflowing exergy still increases although the outflowing chemical exergy of H_2 has a maximum at $\Phi \approx 2.5$ is caused by the decreasing CH_4 conversion and increasing production of high-exergy species such as C_2H_4. The heat and power outputs are significantly lower than the chemical exergies, which slightly decrease with increasing Φ, as already stated before. The exergetic efficiency reaches up to 96% (DME, $\Phi \approx 7$ and DMM, $\Phi \approx 5$), showing that the process is overall favorable. Interestingly, the exergetic efficiency increases with increasing Φ and reaches up to 100% in the case of DMM even though the fuel conversion decreases to nearly 0%. Therefore, it must be noted that the definition of the exergetic efficiency shown in Eq. (6) does not include the exergy loss due to the unconverted fuel. A more robust definition of the exergetic efficiency is the relation of the exergies from the produced syngas and the power and heat outputs to the chemical exergy of the fresh gas ($\eta_{ex}^{mod.} = (\dot{E}_{Syngas} + P + \dot{E}_Q) / \dot{E}_{in}$). According to this definition, the maximum efficiency is 89% at $\Phi \approx 2.5$ but decreases to 27% at $\Phi \approx 5.5$, as also shown in Fig. 9a. The differences in the power, heat, and exergy flows using DME and DMM, respectively, are negligible, as seen from Fig. 9a. However, a deviation appears at $\Phi > 5.5$, which is caused by misfires using DMM as additive whereas the DME/CH_4 mixtures still ignite.

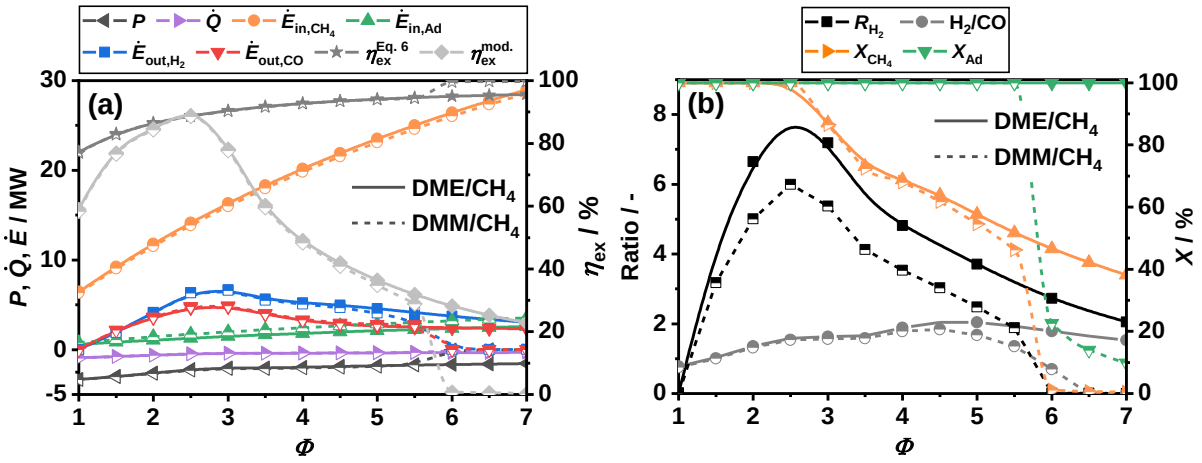

Fig. 9. Power, heat, inlet and outlet exergy flows, H_2 and CO outlet exergy flow (left axis, a), exergetic efficiency (right axis, a), the ratio R_{H2} of produced H_2 to H_2 present in the additive, H_2/CO ratio (left axis, b), and the conversion of CH_4 or additive (right axis, b) as a function of the equivalence ratio at an additive amount of 5% DME (solid lines with filled symbols) or DMM (dashed lines with half-filled symbols). The engine parameters/conditions are: T_0=423 K, d/s=460 mm/580 mm, N=600 min^{-1}. Note that according to thermodynamic conventions, P and $\dot{Q}$ carry a negative sign when transferred from the system.

In Fig. 9b, the produced H_2 related to the H_2 present in the additive (R_{H2}) is given to assess the effectiveness

of additive addition for H_2 production under similar conditions, *i.e.*, T_0=423 K and 5% additive. This ratio should be much larger than 1 to preclude that only the additive is contributing to the syngas production. Results show that a desirable R_{H2} of >1.0 can be obtained in large Φ ranges of 1.3-5.5 and 1.3-9.5, respectively, for DMM/CH_4 and DME/CH_4 mixtures. The model shows the maximum R_{H2} to be up to 7.9 and 6 for DME and DMM, respectively, which is observed at $\Phi \approx 2.5$ due to the maximum syngas yield (see Fig. 9a). At higher Φ, R_{H2} is seen to decrease further because less CH_4 is converted and the product gas composition is slightly shifted towards higher hydrocarbons. Compared to the DME/CH_4 mixtures, the R_{H2} is overall lower for the DMM/CH_4 mixtures since nearly the same amount of H_2 is produced, but more H_2 is introduced by the additive. According to the model, the remaining H_2 in the DMM case is majorly present in H_2O. The H_2/CO ratio lies between 1.0 and 2.0 in a Φ range of up to 4.5, as shown in Fig. 9b. As mentioned before, at higher Φ, the H_2/CO ratio decreases in both cases of DME/CH_4 and DMM/CH_4 and more pronouncedly for the latter.

Overall, the tentative exploration of the methane-fueled polygeneration process with the PolyMech2.1 model shows that both DME and DMM offer promising potential as additives. Although the outputs of interest such as syngas, power, and heat, are slightly reduced if DMM is used as additive, possible soot formation is slightly inhibited. Thus, the operation range can be extended to equivalence ratios of $\Phi > 3$ to produce higher hydrocarbons such as C_2H_4. Regarding the different engines, slow-rotating engines with a high volume-to-surface ratio are preferable since the production of useful chemicals is enhanced due to the longer reaction time and the higher temperatures caused by lower heat losses. Specifically, when the formation of syngas is desired as part of a polygeneration process, an equivalence ratio of 2.5 is shown to be most appropriate under the present assumption, especially for DME as the additive. In contrast, the production of higher hydrocarbons such as C_2H_2, C_2H_4, and C_6H_6 could be favorable at equivalence ratios of 5-7, especially for DMM as the additive. With regard to realistic engine conditions, *i.e.*, knock-free combustion and feasible intake conditions, an intake temperature of 423 K and additive amounts between 2%-5% for DME and 3%-8% for DMM appear to be the most promising conditions for the slow-rotating engine with a high volume-to-surface ratio. In general, the modeling results demonstrate that addition of DME or DMM is very effective in lowering intake temperatures and ensuring ignition even at high equivalence ratios. For future investigations, an optimization could be helpful to find the most interesting conditions using different outputs of interest such as maximum H_2 or C_2H_4 production as the objective function. As already indicated in the

flame results in Section 4.1.2, DME and DMM are both promising fuel additives for the production of C_2 hydrocarbons and formaldehyde, and especially DMM significantly favors the formation of methanol and methyl formate.

It should be noted that the engine simulation results could in principle be affected by uncertainties in thermodynamic data; such effects were found to be negligible, however, when typical uncertainties were taken into account [94, 95]. Only at limited conditions where the ignition timing is very sensitive, would a change of thermodynamic data within the uncertainty range lead to misfires or too early ignition. For all other and thus most conditions, the influence of such uncertainties on the ignition timing and on the mole fractions of product species is negligible so that the conclusions drawn here are not affected. It should also be pointed out that, unlike other experiments, a flame has the uniqueness of a wide temperature range, also found in engines, and is therefore well suited for the investigation of thermo-chemical effects and the validation of thermodynamic and transport data that are important for engine simulations. Detailed discussions on this issue can be found in Section S-VII of SM2.

5. Summary and conclusions

The present study has focused on three main aspects with the aim to explore combinations of DME and DMM with methane in a polygeneration process environment. First, speciation data were obtained in a systematic flame experiment using detailed mass spectrometric investigation of six fuel-rich DME(/CH_4) and DMM(/CH_4) premixed flames. This approach enabled the quantitative measurement of a large number of species, including some value-added chemicals. Second, a comprehensive but compact model (PolyMech2.1) tailored for a polygeneration process involving the DME/DMM/CH_4 fuel system has been developed with the help of these experimental data. This model was then examined against experimental results from the literature, predominantly at high pressure and equivalence ratio >2, covering a considerable range of polygeneration-relevant conditions. Third, parameter studies using this compact model were then performed for generic HCCI engine environments to numerically evaluate the potential and feasibility of a polygeneration process using fuel combinations in the DME/DMM/CH_4 system to flexibly provide valuable products (*e.g.*, syngas), work, and heat.

The flame results showed that CH_4 addition to DME or DMM does not lead to the formation of new species,

and only slightly influences the main consumption pathways of the fuels. Relatively clean syngas can be formed as stable product in the burnt gas for the flames at richer conditions (Φ=1.7) with high yields of, *e.g.*, up to ~78% CO and ~35% H_2 in the 62%DME/38%CH_4 flame. Among the large number of C_1-C_4 hydrocarbon and oxygenated intermediates detected, acetylene, ethylene, ethane, and formaldehyde are dominant ones with peak yields of 2.1%-8.7%. Interestingly, methanol and methyl formate also showed comparably high yields of up to 0.6%-6.7%, but only in the flames with DMM.

The developed model is shown to satisfactorily reproduce both the obtained flame data in this study and a large literature dataset at engine-like or polygeneration-relevant conditions ($\Phi \geq 2$ and elevated pressure). Importantly, as a compact model, PolyMech2.1 showed the advantage of significantly decreased simulation times in an HCCI engine environment compared to typical previous models, *e.g.*, by a factor of 20 compared to the Jacobs model (Jacobs et al., *Combust & Flame* 205 (2019) 522-533) using a single-zone model.

The model-assisted parameter study of the generic engine types showed, for both DME and DMM, promising potential as additives for a methane-fueled polygeneration process. For example, the simulation results showed that with 18% DME addition to CH_4, the syngas yield can reach up to 77% at Φ=3 while maintaining a high CH_4 conversion of 99%. DMM addition to CH_4 exhibited slightly lower syngas yield in comparison to DME in both the flame and engine simulations, whereas it showed decreased sooting propensity in comparison to DME, even at a Φ of >3. According to these results, the operation range might be extended to richer condition by using DMM as fuel additive if the production of valuable chemicals such as C_2 hydrocarbons is targeted. Furthermore, the simulation predicted low-rotating engines with a high volume-to-surface ratio to be preferable since the production of useful chemicals is enhanced due to the longer reaction time and the higher temperatures caused by lower heat losses. The corresponding exergetic analysis of a polygeneration process in such an engine environment using the DME/DMM/CH_4 fuel system suggested an exergetic efficiency of up to 96%, underlining the potential promise of this process.

Acknowledgement

HZ is grateful for a fellowship of the Alexander von Humboldt (AvH) Foundation that has supported his research at Bielefeld University and German Aerospace Center (DLR). Financial support for the work performed by CR, DK, TK, and BA by the Deutsche Forschungsgemeinschaft (DFG) within the framework

of the DFG research unit FOR 1993 “Multifunctional conversion of chemical species and energy” (Project number 229243862) is also gratefully acknowledged. NG, PO, and TB thank DLR for financial support within the framework of the DLR internal project “Future Fuels”.

Credit author statement

HZ: Investigation, Formal Analysis, Writing - Original draft preparation
DK: Investigation, Formal Analysis, Writing - Original draft preparation
CR: Investigation, Formal Analysis, Writing - Original draft preparation
SS: Investigation, Validation, Visualization, Writing-Review and editing
NG: Investigation, Writing-Review and editing
PO: Investigation, Validation, Supervision, Writing-Review and editing
TB: Investigation, Writing-Review and editing
TK: Conceptualization, Supervision, Project administration, Writing-Review and editing
BA: Conceptualization, Supervision, Project administration, Writing-Review and editing
KKH: Conceptualization, Supervision, Project administration, Writing-Review and editing

References

[1] D. Schroeder, R. Hegner, A. Güngör, B. Atakan, Exergoeconomic analysis of an HCCI engine polygeneration process, Energy Convers. Manag. 203 (2020) 112085.

[2] B. Atakan, S.A. Kaiser, J. Herzler, S. Porras, K. Banke, O. Deutschmann, T. Kasper, M. Fikri, R. Schießl, D. Schröder, Flexible energy conversion and storage via high-temperature gas-phase reactions: The piston engine as a polygeneration reactor, Renew. Sustain. Energy Rev. 133 (2020) 110264.

[3] K. Jana, A. Ray, M.M. Majoumerd, M. Assadi, S. De, Polygeneration as a future sustainable energy solution–A comprehensive review, Appl. Energy 202 (2017) 88-111.

[4] H. Gossler, O. Deutschmann, Numerical optimization and reaction flow analysis of syngas production via partial oxidation of natural gas in internal combustion engines, Int. J. Hydrog. Energy 40 (2015) 11046-11058.

[5] R. Hegner, B. Atakan, A polygeneration process concept for HCCI-engines–Modeling product gas purification and exergy losses, Int. J. Hydrog. Energy 42 (2017) 1287-1297.

[6] R. Hegner, M. Werler, R. Schießl, U. Maas, B. Atakan, Fuel-Rich HCCI engines as chemical reactors for polygeneration: A modeling and experimental study on product species and thermodynamics, Energy Fuels 31 (2017) 14079-14088.

[7] K. Banke, R. Hegner, D. Schröder, C. Schulz, B. Atakan, S. Kaiser, Power and syngas production from partial oxidation of fuel-rich methane/DME mixtures in an HCCI engine, Fuel 243 (2019) 97-103.

[8] T. Korakianitis, A. Namasivayam, R. Crookes, Natural-gas fueled spark-ignition (SI) and compression-ignition (CI) engine performance and emissions, Prog. Energy Combust. Sci. 37 (2011) 89-112.

[9] D. Kaczmarek, J. Herzler, S. Porras, S. Shaqiri, M. Fikri, C. Schulz, B. Atakan, U. Maas, T. Kasper, Plug-flow reactor and shock-tube study of the oxidation of very fuel-rich natural gas/DME/O_2 mixtures, Combust. Flame 225 (2021) 86-103.

[10] C.B. Reuter, R. Zhang, O.R. Yehia, Y. Rezgui, Y. Ju, Counterflow flame experiments and chemical kinetic modeling of dimethyl ether/methane mixtures, Combust. Flame 196 (2018) 1-10.

[11] Z. Wang, L. Yang, B. Li, Z. Li, Z. Sun, M. Aldén, K. Cen, A. Konnov, Investigation of combustion enhancement by ozone additive in CH_4/air flames using direct laminar burning velocity measurements and kinetic simulations, Combust. Flame 159 (2012) 120-129.

[12] D. Schröder, K. Banke, S.A. Kaiser, B. Atakan, The kinetics of methane ignition in fuel-rich HCCI engines: DME replacement by ozone, Proc. Combust. Inst. 38 (2020) 5567-5574.

[13] D. Kaczmarek, B. Atakan, T. Kasper, Investigation of the partial oxidation of methane/*n*-heptane-mixtures and the interaction of methane and n-heptane under ultra-rich conditions, Combust. Flame 205 (2019) 345-357.

[14] J. Herzler, M. Fikri, C. Schulz, High-pressure shock-tube study of the ignition and product formation of fuel-rich dimethoxymethane (DMM)/air and CH_4/DMM/air mixtures, Combust. Flame 216 (2020) 293-299.

[15] A. Omari, B. Heuser, S. Pischinger, C. Rüdinger, Potential of long-chain oxymethylene ether and oxymethylene ether-diesel blends for ultra-low emission engines, Appl. Energy 239 (2019) 1242-1249.

[16] L. Cai, S. Jacobs, R. Langer, F. vom Lehn, K.A. Heufer, H. Pitsch, Auto-ignition of oxymethylene ethers (OME_n, n=2-4) as promising synthetic e-fuels from renewable electricity: shock tube experiments and automatic mechanism generation, Fuel 264 (2020) 116711.

[17] W. Sun, G. Wang, S. Li, R. Zhang, B. Yang, J. Yang, Y. Li, C.K. Westbrook, C.K. Law, Speciation and the laminar burning velocities of poly (oxymethylene) dimethyl ether 3 (POMDME3) flames: An experimental and modeling study, Proc. Combust. Inst. 36 (2017) 1269-1278.

[18] A. García, A. Gil, J. Monsalve-Serrano, R.L. Sari, OME_x-diesel blends as high reactivity fuel for ultra-low NO_x and soot emissions in the dual-mode dual-fuel combustion strategy, Fuel 275 (2020) 117898.

[19] W. Lowry, Z. Serinyel, M. Krejci, H. Curran, G. Bourque, E. Petersen, Effect of methane-dimethyl ether fuel blends on flame stability, laminar flame speed, and Markstein length, Proc. Combust. Inst. 33 (2011) 929-937.

[20] C. Tang, L. Wei, J. Zhang, X. Man, Z. Huang, Shock tube measurements and kinetic investigation on the ignition delay times of methane/dimethyl ether mixtures, Energy Fuels 26 (2012) 6720-6728.

[21] H. Yu, E. Hu, Y. Cheng, X. Zhang, Z. Huang, Experimental and numerical study of laminar premixed dimethyl ether/methane–air flame, Fuel 136 (2014) 37-45.

[22] U. Burke, K.P. Somers, P. O'Toole, C.M. Zinner, N. Marquet, G. Bourque, E.L. Petersen, W.K. Metcalfe, Z. Serinyel, H.J. Curran, An ignition delay and kinetic modeling study of methane, dimethyl ether, and their mixtures at high pressures, Combust. Flame 162 (2015) 315-330.

[23] F. Sen, B. Shu, T. Kasper, J. Herzler, O. Welz, M. Fikri, B. Atakan, C. Schulz, Shock-tube and plug-flow reactor study of the oxidation of fuel-rich CH_4/O_2 mixtures enhanced with additives, Combust. Flame 169 (2016) 307-320.

[24] Y. Kang, W. Shuang, X. Jiang, Y. Song, S. Sun, P. Zhang, Y. Sun, X. Lu, Q. Wang, X. Gou, Study on effect of dimethyl ether addition on combustion characteristics of turbulent methane/air jet diffusion flame, Fuel Process. Technol. 159 (2017) 421-435.

[25] Z. Wang, S. Wang, R. Whiddon, X. Han, Y. He, K. Cen, Effect of hydrogen addition on laminar burning velocity of CH_4/DME mixtures by heat flux method and kinetic modeling, Fuel 232 (2018) 729-742.

[26] H. Hashemi, J.M. Christensen, P. Glarborg, High-pressure pyrolysis and oxidation of DME and DME/CH_4, Combust. Flame 205 (2019) 80-92.

[27] A. Mohammad, K.A. Juhany, Laminar burning velocity and flame structure of DME/methane+air mixtures at elevated temperatures, Fuel 245 (2019) 105-114.

[28] S. Porras, D. Kaczmarek, J. Herzler, S. Drost, M. Werler, T. Kasper, M. Fikri, R. Schießl, B. Atakan, C. Schulz, An experimental and modeling study on the reactivity of extremely fuel-rich methane/dimethyl ether mixtures,

Combust. Flame 212 (2020) 107-122.

[29] D. Kaczmarek, J. Herzler, S. Porras, S. Shaqiri, M. Fikri, C. Schulz, B. Atakan, U. Maas, T. Kasper, Plug-flow reactor and shock-tube study of the oxidation of very fuel-rich natural gas/DME/O_2 mixtures, Combust. Flame 225 (2021) 86-103.

[30] H. Nakamura, T. Sugita, T. Tezuka, K. Maruta, Study on methane oxidation affected by dimethyl ether oxidation at low temperatures using a micro flow reactor with a controlled temperature profile, Combust. Flame 223 (2021) 320-329.

[31] J. Li, A. Tang, T. Cai, C. Zhou, Effect of dimethyl ether addition on flame stability of premixed methane/air in a micro-planar quartz combustor, Chem. Eng. Process. 147 (2020) 107740.

[32] J. Luo, W. Li, L. Tian, L. Liu, Experimental and numerical study of oxygen diluted partially premixed dimethyl ether/methane counter flow flame, Chem. Eng. Trans. 61 (2017) 415-420.

[33] S. Yoon, D. Anh, S. Chung, Synergistic effect of mixing dimethyl ether with methane, ethane, propane, and ethylene fuels on polycyclic aromatic hydrocarbon and soot formation, Combust. Flame 154 (2008) 368-377.

[34] T. Bierkandt, P. Oßwald, N. Gaiser, D. Krüger, M. Köhler, M. Hoener, S. Shaqiri, D. Kaczmarek, Y. Karakaya, P. Hemberger, Observation of low-temperature chemistry products in laminar premixed low-pressure flames by molecular-beam mass spectrometry, Int. J. Chem. Kinet. 53 (2021) 1063-1081.

[35] P. Oßwald, P. Hemberger, T. Bierkandt, E. Akyildiz, M. Köhler, A. Bodi, T. Gerber, T. Kasper, In situ flame chemistry tracing by imaging photoelectron photoion coincidence spectroscopy, Rev. Sci. Instrum. 85 (2014) 025101.

[36] N. Hansen, T.A. Cool, P.R. Westmoreland, K. Kohse-Höinghaus, Recent contributions of flame-sampling molecular-beam mass spectrometry to a fundamental understanding of combustion chemistry, Prog. Energy Combust. Sci. 35 (2009) 168-191.

[37] D. Liu, J. Santner, C. Togbé, D. Felsmann, J. Koppmann, A. Lackner, X. Yang, X. Shen, Y. Ju, K. Kohse-Höinghaus, Flame structure and kinetic studies of carbon dioxide-diluted dimethyl ether flames at reduced and elevated pressures, Combust. Flame 160 (2013) 2654-2668.

[38] H. Xu, C. Yao, T. Yuan, K. Zhang, H. Guo, Measurements and modeling study of intermediates in ethanol and dimethy ether low-pressure premixed flames using synchrotron photoionization, Combust. Flame 158 (2011) 1673-1681.

[39] T.A. Cool, J. Wang, N. Hansen, P.R. Westmoreland, F.L. Dryer, Z. Zhao, A. Kazakov, T. Kasper, K. Kohse-Höinghaus, Photoionization mass spectrometry and modeling studies of the chemistry of fuel-rich dimethyl ether flames, Proc. Combust. Inst. 31 (2007) 285-293.

[40] W. Sun, B. Yang, N. Hansen, K. Moshammer, The influence of dimethoxy methane (DMM)/dimethyl carbonate (DMC) addition on a premixed ethane/oxygen/argon flame, Proc. Combust. Inst. 36 (2017) 449-457.

[41] A. Mcilroy, T.D. Hain, H.A. Michelsen, T.A. Cool, A laser and molecular beam mass spectrometer study of low-pressure dimethyl ether flames, Proc. Combust. Inst. 28 (2000) 1647-1653.

[42] L.-S. Tran, P.-A. Glaude, R. Fournet, F. Battin-Leclerc, Experimental and modeling study of premixed laminar flames of ethanol and methane, Energy Fuels 27 (2013) 2226-2245.

[43] C.-W. Zhou, Y. Li, U. Burke, C. Banyon, K.P. Somers, S. Ding, S. Khan, J.W. Hargis, T. Sikes, O. Mathieu, An experimental and chemical kinetic modeling study of 1, 3-butadiene combustion: Ignition delay time and laminar flame speed measurements, Combust. Flame 197 (2018) 423-438.

[44] S. Jacobs, M. Döntgen, A.B. Alquaity, W.A. Kopp, L.C. Kröger, U. Burke, H. Pitsch, K. Leonhard, H.J. Curran, K.A. Heufer, Detailed kinetic modeling of dimethoxymethane. Part II: Experimental and theoretical study of the kinetics and reaction mechanism, Combust. Flame 205 (2019) 522-533.

[45] B. Crunelle, D. Surdyk, J. Pauwels, L. Sochet, Experimental study of low-pressure premixed methane and ethane flames by molecular beam sampling and mass spectrometry analysis, J. Chim. Phys 94 (1997) 433-459.

[46] R. Hennessy, C. Robinson, D. Smith, A comparative study of methane and ethane flame chemistry by experiment and detailed modelling, Symp. (Int.) Combust. 22 (1988) 761-772.

[47] M. Musick, P. Van Tiggelen, J. Vandooren, Experimental study of the structure of several fuel-rich premixed flames of methane, oxygen, and argon, Combust. Flame 105 (1996) 433-450.

[48] C. Langley, A. Burgess, A study of premixed fuel-rich methane flames by molecular beam mass spectrometry: the primary reaction zone, Proc. R. Soc. A 421 (1989) 259-278.

[49] L. Seidel, K. Moshammer, X. Wang, T. Zeuch, K. Kohse-Höinghaus, F. Mauss, Comprehensive kinetic modeling and experimental study of a fuel-rich, premixed *n*-heptane flame, Combust. Flame 162 (2015) 2045-2058.

[50] M. Schenk, L. Leon, K. Moshammer, P. Oßwald, T. Zeuch, L. Seidel, F. Mauss, K. Kohse-Höinghaus, Detailed mass spectrometric and modeling study of isomeric butene flames, Combust. Flame 160 (2013) 487-503.

[51] J.C. Biordi, Molecular beam mass spectrometry for studying the fundamental chemistry of flames, Prog. Energy Combust. Sci. 3 (1977) 151-173.

[52] U. Struckmeier, P. Oßwald, T. Kasper, L. Böhling, M. Heusing, M. Köhler, A. Brockhinke, K. Kohse-Höinghaus, Sampling probe influences on temperature and species concentrations in molecular beam mass spectroscopic investigations of flat premixed low-pressure flames, Z. Phys. Chem. 223 (2009) 503-537.

[53] N. Bahlawane, U. Struckmeier, T.S. Kasper, P. Oßwald, Noncatalytic thermocouple coatings produced with chemical vapor deposition for flame temperature measurements, Rev. Sci. Instrum., 78 (2007) 013905.

[54] C.R. Shaddix, Correcting thermocouple measurements for radiation loss: a critical review, 33rd National Heat Transfer Conference (1999).

[55] X. Yang, D. Felsmann, N. Kurimoto, J. Krüger, T. Wada, T. Tan, E.A. Carter, K. Kohse-Höinghaus, Y. Ju, Kinetic studies of methyl acetate pyrolysis and oxidation in a flow reactor and a low-pressure flat flame using molecular-beam mass spectrometry, Proc. Combust. Inst. 35 (2015) 491-498.

[56] F.N. Egolfopoulos, N. Hansen, Y. Ju, K. Kohse-Höinghaus, C.K. Law, F. Qi, Advances and challenges in laminar flame experiments and implications for combustion chemistry, Prog. Energy Combust. Sci. 43 (2014) 36-67.

[57] CHEMKIN-PRO R1, Reaction Design: San Diego, 2020.

[58] T. He, Z. Wang, X. You, H. Liu, Y. Wang, X. Li, X. He, A chemical kinetic mechanism for the low-and intermediate-temperature combustion of Polyoxymethylene Dimethyl Ether 3 (PODE3), Fuel 212 (2018) 223-235.

[59] F.H. Vermeire, H.-H. Carstensen, O. Herbinet, F. Battin-Leclerc, G.B. Marin, K.M. Van Geem, Experimental and modeling study of the pyrolysis and combustion of dimethoxymethane, Combust. Flame 190 (2018) 270-283.

[60] Y. Wu, S. Panigrahy, A.B. Sahu, C. Bariki, J. Beeckmann, J. Liang, A.A. Mohamed, S. Dong, C. Tang, H. Pitsch, Understanding the antagonistic effect of methanol as a component in surrogate fuel models: A case study of methanol/n-heptane mixtures, Combust. Flame 226 (2021) 229-242.

[61] R.M. Vichietti, F.B. Machado, R.L. Haiduke, Accurate rate constants for the forward and reverse H+ CO↔ HCO reactions at the high-pressure Limit, ACS Omega 5 (2020) 23975-23982.

[62] Z. Xu, P. Raghunath, M.-C. Lin, *Ab Initio* chemical kinetics for the CH_3+O (3P) reaction and related isomerization–decomposition of CH_3O and CH_2OH radicals, J. Phys. Chem. A 119 (2015) 7404-7417.

[63] J. Li, Z. Zhao, A. Kazakov, M. Chaos, F.L. Dryer, J.J. Scire Jr, A comprehensive kinetic mechanism for CO,

CH_2O, and CH_3OH combustion, Int. J. Chem. Kinet. 39 (2007) 109-136.

[64] L.B. Harding, S.J. Klippenstein, Y. Georgievskii, Reactions of oxygen atoms with hydrocarbon radicals: a priori kinetic predictions for the CH_3+O, C_2H_5+O, and C_2H_3+O reactions, Proc. Combust. Inst. 30 (2005) 985-993.

[65] P.W. Seakins, S.R. Leone, A laser flash photolysis/time-resolved FTIR emission study of a new channel in the reaction of methyl+ oxygen atom: production of carbon monoxide (v), J. Phys. Chem. 96 (1992) 4478-4485.

[66] W. Hack, M. Hold, K. Hoyermann, J. Wehmeyer, T. Zeuch, Mechanism and rate of the reaction CH_3+O—revisited, Phys. Chem. Chem. Phys. 7 (2005) 1977-1984.

[67] R.S. Tranter, P.T. Lynch, C.J. Annesley, Shock tube investigation of CH_3+CH_3OCH_3, J. Phys. Chem. A 116 (2012) 7287-7292.

[68] C.F. Goldsmith, L.B. Harding, Y. Georgievskii, J.A. Miller, S.J. Klippenstein, Temperature and pressure-dependent rate coefficients for the reaction of vinyl radical with molecular oxygen, J. Phys. Chem. A 119 (2015) 7766-7779.

[69] T.L. Nguyen, L. Vereecken, J. Peeters, Quantum chemical and theoretical kinetics study of the $O(^3P)$+C_2H_2 reaction: a multistate process, J. Phys. Chem. A 110 (2006) 6696-6706.

[70] A.W. Jasper, S.J. Klippenstein, L.B. Harding, B. Ruscic, Kinetics of the reaction of methyl radical with hydroxyl radical and methanol decomposition, J. Phys. Chem. A 111 (2007) 3932-3950.

[71] R. Sivaramakrishnan, M.-C. Su, J. Michael, S. Klippenstein, L. Harding, B. Ruscic, Shock tube and theoretical studies on the thermal decomposition of propane: evidence for a roaming radical channel, J. Phys. Chem. A 115 (2011) 3366-3379.

[72] R. Sivaramakrishnan, J.V. Michael, A.F. Wagner, R. Dawes, A.W. Jasper, L.B. Harding, Y. Georgievskii, S.J. Klippenstein, Roaming radicals in the thermal decomposition of dimethyl ether: Experiment and theory, Combust. Flame 158 (2011) 618-632.

[73] J.A. Miller, S.J. Klippenstein, The recombination of propargyl radicals and other reactions on a C_6H_6 potential, J. Phys. Chem. A 107 (2003) 7783-7799.

[74] J.-G. Chang, H.-T. Chen, S. Xu, M.-C. Lin, Computational study on the kinetics and mechanisms for the unimolecular decomposition of formic and oxalic acids, J. Phys. Chem. A 111 (2007) 6789-6797.

[75] W. Sun, T. Tao, M. Lailliau, N. Hansen, B. Yang, P. Dagaut, Exploration of the oxidation chemistry of dimethoxymethane: Jet-stirred reactor experiments and kinetic modeling, Combust. Flame 193 (2018) 491-501.

[76] D. Goodwin, H. Moffat, R.L. Speth, Cantera: An object-oriented software toolkit for chemical kinetics, thermodynamics, and transport processes, 2009.

[77] J.B. Heywood, Internal combustion engine fundamentals, McGraw-Hill Education, New York, United States, 2018.

[78] C. Rudolph, B. Atakan, Investigation of natural gas/hydrogen mixtures for exergy storage in a piston engine, Energy, 218 (2021) 119375.

[79] J. Chang, O. Güralp, Z. Filipi, D. Assanis, T.-W. Kuo, P. Najt, R. Rask, New heat transfer correlation for an HCCI engine derived from measurements of instantaneous surface heat flux, SAE Transactions (2004) 1576-1593.

[80] N. Komninos, Assessing the effect of mass transfer on the formation of HC and CO emissions in HCCI engines, using a multi-zone model, Energy Convers. Manag. 50 (2009) 1192-1201.

[81] D. Freund, B. Atakan, Ozone and dimethyl ether in fuel-rich HCCI engines: an exergetic evaluation, 10th European Combustion Meeting (2021).

[82] X. Jiang, W. Huang, H.J.F. Zhao, Ignition delay times of iso-butane activated by DME under various equivalence ratios in the shock tube, Fuel 287 (2021) 119486.

[83] J. Wullenkord, I. Graf, M. Baroncelli, D. Felsmann, L. Cai, H. Pitsch, K.J.C. Kohse-Höinghaus, Flame, Laminar premixed and non-premixed flame investigation on the influence of dimethyl ether addition on *n*-heptane combustion, Combust. Flame 212 (2020) 323-336.

[84] M. Zeng, J. Wullenkord, I. Graf, K. Kohse-Höinghaus, Influence of dimethyl ether and diethyl ether addition on the flame structure and pollutant formation in premixed iso-octane flames, Combust. Flame 184 (2017) 41-54.

[85] J. Wang, M. Chaos, B. Yang, T.A. Cool, F.L. Dryer, T. Kasper, N. Hansen, P. Oßwald, K. Kohse-Höinghaus, P.R. Westmoreland, Composition of reaction intermediates for stoichiometric and fuel-rich dimethyl ether flames: flame-sampling mass spectrometry and modeling studies, Phys. Chem. Chem. Phys. 11 (2009) 1328-1339.

[86] H. Zhang, S. Schmitt, L. Ruwe, K. Kohse-Höinghaus, Inhibiting and promoting effects of NO on dimethyl ether and dimethoxymethane oxidation in a plug-flow reactor, Combust. Flame 224 (2021) 94-107.

[87] V. Dias, X. Lories, J. Vandooren, Lean and rich premixed dimethoxymethane/oxygen/argon flames: experimental and modeling, Combust. Sci. Technol. 182 (2010) 350-364.

[88] N. Gaiser, T. Bierkandt, P. Oßwald, J. Zinsmeister, T. Kathrotia, S. Shaqiri, P. Hemberger, T. Kasper, M. Aigner, M. Köhler: Oxidation of oxymethylene ether (OME0-5): An experimental systematic study by mass spectrometry and photoelectron photoion coincidence spectroscopy, submitted to Fuel, 2021.

[89] V. Dias, C. Renard, J. Vandooren, Modeling of rich premixed C_2H_4/O_2/Ar and C_2H_4/dimethoxymethane/O_2/Ar flames, Z. Phys. Chem. 223 (2009) 565.

[90] C. Renard, P. Van Tiggelen, J. Vandooren, Effect of dimethoxymethane addition on the experimental structure of a rich ethylene/oxygen/argon flame, Proc. Combust. Inst. 29 (2002) 1277-1284.

[91] R. Sun, I. Delidovich, R. Palkovits, Dimethoxymethane as a cleaner synthetic fuel: synthetic methods, catalysts, and reaction mechanism, ACS Catal. 9 (2019) 1298-1318.

[92] A.T. To, T.J. Wilke, E. Nelson, C.P. Nash, A. Bartling, E.C. Wegener, K.A. Unocic, S.E. Habas, T.D. Foust, D.A. Ruddy, Dehydrogenative coupling of methanol for the gas-phase, one-step synthesis of dimethoxymethane over supported copper catalysts, ACS Sustain. Chem. Eng. 8 (2020) 12151-12160.

[93] H. Nazir, N. Muthuswamy, C. Louis, S. Jose, J. Prakash, M.E. Buan, C. Flox, S. Chavan, X. Shi, P. Kauranen, Is the H_2 economy realizable in the foreseeable future? Part III: H_2 usage technologies, applications, and challenges and opportunities, Int. J. Hydrog. Energy 45 (2020) 28217-28239.

[94] ATcT Thermochemical Values (ver. 1.122p), Argonne National Laboratory, https://atct.anl.gov/Thermochemical%20Data/version%201.122p/index.php#ref_1

[95] W.A. Kopp, L.C. Kröger, M. Döntgen, S. Jacobs, U. Burke, H.J. Curran, K.A. Heufer, K. Leonhard, Detailed kinetic modeling of dimethoxymethane. Part I: Ab initio thermochemistry and kinetics predictions for key reactions, Combust. Flame 189 (2018) 433-442.